Cell Metabolism

A PRDM16-Driven Metabolic Signal from Adipocytes Regulates Precursor Cell Fate

Graphical Abstract
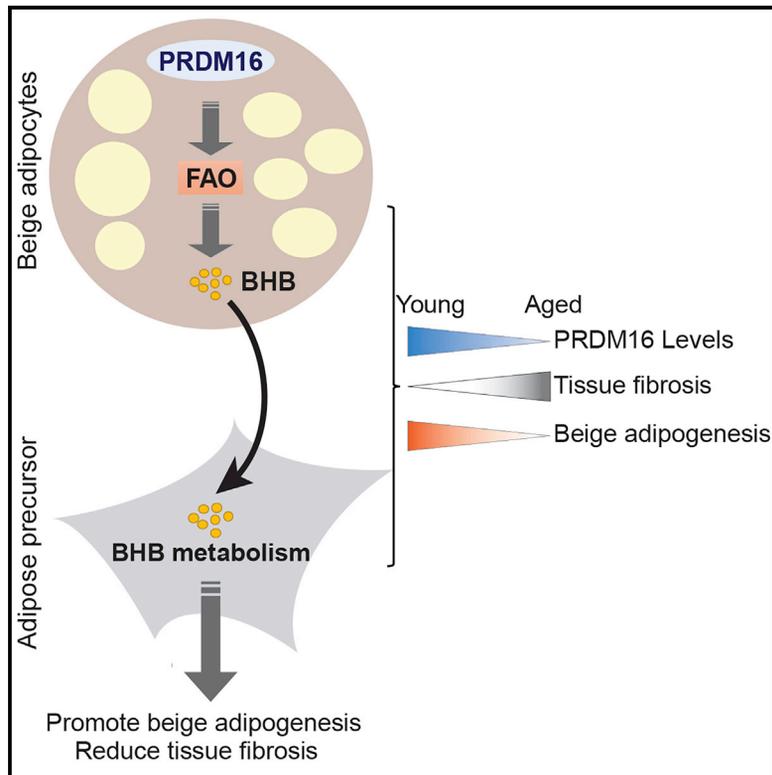
Authors

Wenshan Wang, Jeff Ishibashi,
Sophie Trefely, ..., Nathaniel W. Snyder,
Rana K. Gupta, Patrick Seale

Correspondence

sealep@pennmedicine.upenn.edu

In Brief

Wang et al. show that mature adipocytes secrete beta-hydroxybutyrate (BHB), which acts on adipose precursor cells to suppress fibrosis responses and facilitate beige adipocyte differentiation. Raising BHB levels ameliorates adipose fibrosis and restores beige fat development in aged animals.

Highlights

- Beiging stimuli decrease the fibrotic phenotype of adipose precursor cells

- Aging reduces adipocyte PRDM16 expression and impairs beige fat remodeling

- PRDM16 induces beta-hydroxybutyrate (BHB) secretion from adipocytes

- Metabolism of BHB in precursor cells blocks fibrosis and enhances beige adipogenesis

CellPress

A PRDM16-Driven Metabolic Signal from Adipocytes Regulates Precursor Cell Fate

Wenshan Wang,[1,2] Jeff Ishibashi,[1,2] Sophie Trefely,[3,6] Mengle Shao,[7] Alexis J. Cowan,[8] Alexander Sakers,[1,2]
Hee-Woong Lim,[1,4] Sean O'Connor,[9] Mary T. Doan,[6] Paul Cohen,[9] Joseph A. Baur,[1,5] M. Todd King,[10] Richard L. Veech,[10]
Kyoung-Jae Won,[1,4] Joshua D. Rabinowitz,[8] Nathaniel W. Snyder,[6] Rana K. Gupta,[7] and Patrick Seale[1,2,11,*]

[1]Institute for Diabetes, Obesity & Metabolism, University of Pennsylvania, Philadelphia, PA, USA
[2]Department of Cell and Developmental Biology, University of Pennsylvania, Philadelphia, PA, USA
[3]Department of Cancer Biology, University of Pennsylvania Philadelphia, PA, USA
[4]Genetics Department, University of Pennsylvania, Philadelphia, PA, USA
[5]Department of Physiology, Perelman School of Medicine, University of Pennsylvania, Philadelphia, PA, USA
[6]AJ Drexel Autism Institute, Drexel University, Philadelphia, PA, USA
[7]Touchstone Diabetes Center, Department of Internal Medicine, University of Texas Southwestern Medical Center, Dallas, TX, USA
[8]Lewis-Sigler Institute for Integrative Genomics and Department of Chemistry, Princeton University, Princeton, NJ, 08544 USA
[9]Laboratory of Molecular Metabolism, The Rockefeller University, New York, NY, USA
[10]Laboratory of Metabolic Control, NIH/NIAAA, Rockville, MD, USA
[11]Lead Contact
*Correspondence: sealep@pennmedicine.upenn.edu
https://doi.org/10.1016/j.cmet.2019.05.005

SUMMARY

The precursor cells for metabolically beneficial beige adipocytes can alternatively become fibrogenic and contribute to adipose fibrosis. We found that cold exposure or β3-adrenergic agonist treatment of mice decreased the fibrogenic profile of precursor cells and stimulated beige adipocyte differentiation. This fibrogenic-to-adipogenic transition was impaired in aged animals, correlating with reduced adipocyte expression of the transcription factor PRDM16. Genetic loss of *Prdm16* mimicked the effect of aging in promoting fibrosis, whereas increasing PRDM16 in aged mice decreased fibrosis and restored beige adipose development. PRDM16-expressing adipose cells secreted the metabolite β-hydroxybutyrate (BHB), which blocked precursor fibrogenesis and facilitated beige adipogenesis. BHB catabolism in precursor cells, mediated by BDH1, was required for beige fat differentiation *in vivo*. Finally, dietary BHB supplementation in aged animals reduced adipose fibrosis and promoted beige fat formation. Together, our results demonstrate that adipocytes secrete a metabolite signal that controls beige fat remodeling.

INTRODUCTION

Brown and beige adipocytes burn energy for heat production and have garnered much attention because of their capacity to counteract metabolic disease (Harms and Seale, 2013; Kajimura et al., 2015). Brown adipocytes are located in discrete deposits of brown adipose tissue (BAT), whereas beige adipocytes develop in white adipose tissue (WAT) in response to environmental cold and other stimuli (Wang and Seale, 2016). Brown and beige adipocytes have abundant mitochondria that contain uncoupling protein 1 (UCP1) (Cannon and Nedergaard, 2004). Upon activation by cold or β-adrenergic signaling, UCP1 catalyzes proton leak across the inner mitochondrial membrane, resulting in increased oxygen consumption and heat production (Cannon and Nedergaard, 2004; Fedorenko et al., 2012; Klingenberg and Huang, 1999; Ricquier, 2011).

Increasing the amount and/or activity of beige adipocytes in mice promotes a lean and healthy metabolic phenotype (Wu et al., 2013). Conversely, reductions in beige fat activity predispose animals to the harmful metabolic effects of a high-fat diet (Cohen et al., 2014). Beige adipocytes develop from

Context and Significance

Beige fat cells burn energy and can thereby reduce obesity and metabolic disease. The precursor cells that develop into beige fat also give rise to fibrosis-generating cells that contribute to metabolic dysfunction. This study shows that mature fat cells produce a metabolic signal, β hydroxybutyrate (BHB), which acts on precursor cells to repress fibrosis and stimulate beige fat development. The production of BHB by fat cells is controlled by the regulatory protein PRDM16. PRDM16 and BHB levels decline in fat tissue during aging, resulting in fibrosis and diminished beige fat. Dietary supplementation of BHB in aged mice decreases fibrosis and restores beige fat formation, raising the possibility that this pathway could be targeted therapeutically to reduce obesity.
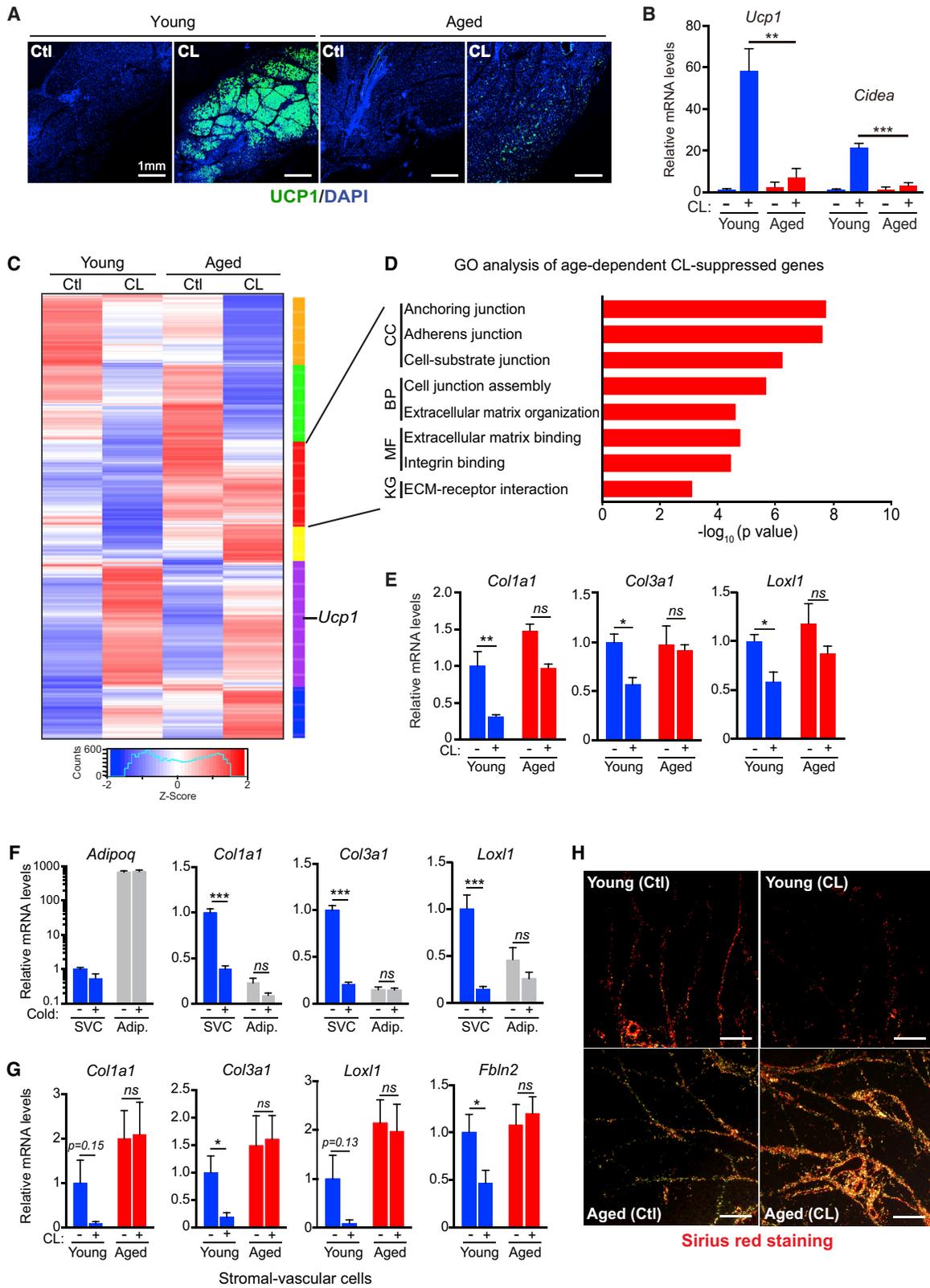
Figure 1. Cold or β3 Agonism Induces a Fibrogenic-to-Adipogenic Phenotypic Shift in Adipose Stromal Cells

(A–E) Young (2-month-old) and aged (12-month-old) mice were acclimated to thermoneutrality and treated with vehicle or CL for 4 days to induce beiging.

(A) Immunofluorescence staining for UCP1 (green) in iWAT. Nuclei (DAPI, blue); scale bar, 1 mm.

(legend continued on next page)

PDGFRα+ precursor cells that are also capable of differentiating into fibrosis-inducing myofibroblast cells (Berry et al., 2016; Lee et al., 2012; Lin et al., 2018; Long et al., 2014; Marcelin et al., 2017; McDonald et al., 2015; Shao et al., 2016; Wang et al., 2013). Analogous mesenchymal cell populations possessing adipogenic and fibrogenic potential, called fibro-adipogenic progenitor (FAP) cells, are also present in skeletal muscle and heart (Joe et al., 2010; Lemos et al., 2015; Uezumi et al., 2010).

Myofibroblast differentiation in adipose tissue is stimulated by various pathways, including hypoxia/HIF1α and TGFβ (Halberg et al., 2009; Marcelin et al., 2017; Sun et al., 2013a, 2013b; Vila et al., 2014). HIF1α activation in adipose tissue is sufficient to trigger fibrosis, whereas pharmacological inhibition of HIF1α reduces fibrosis and improves systemic metabolism (Halberg et al., 2009; Jiang et al., 2011; Sun et al., 2013a). TGFβ promotes fibrogenesis through activation of Rho-associated protein kinase (ROCK) and resultant assembly of actin stress fibers (Carthy, 2018). Notably, deletion of *Mrtfa*, a downstream effector in the TGFβ pathway, blocks the myofibrogenic programming of adipose precursors and facilitates beige fat differentiation (Lin et al., 2018; McDonald et al., 2015). However, the upstream signals that regulate the fibrogenic versus adipogenic activity of precursor cells during beige fat development are yet unknown.

The zinc-finger transcriptional factor PRD1-BF1-RIZ1 homologous domain-containing protein 16 (PRDM16) is a powerful driver of brown and beige adipocyte identity (Cohen et al., 2014; Harms et al., 2015; Ishibashi and Seale, 2015; Kajimura et al., 2008; Ohno et al., 2013; Seale et al., 2007, 2011). PRDM16 co-activates PPARγ and PPARα in adipocytes to activate the expression of thermogenic genes (Hondares et al., 2011; Seale et al., 2008). Interestingly, PRDM16 overexpression in adipose tissue reduces high-fat-diet-induced fibrosis (Hasegawa et al., 2018). However, if and how PRDM16 action in adipocytes affects the fibrogenic versus beige adipogenic fate of precursor cells was unclear.

In this study, we identify a PRDM16-regulated adipocyte-to-precursor paracrine signal that suppresses fibrogenesis and facilitates beige fat development. Specifically, PRDM16 drives a fatty acid oxidation and ketogenesis program in adipose cells, leading to secretion of the metabolite β-hydroxybutyrate (BHB). BHB acts on precursor cells to block HIF1α- or TGFβ-induced myofibroblast differentiation and promote beige adipocyte differentiation. This action of BHB in precursor cells is dependent on the ketolytic enzyme BDH1, revealing an important role for ketone metabolism in adipose tissue remodeling. Finally, raising PRDM16 or BHB levels in mice reverses aging-induced fibrosis and restores beige fat developmental potential.

RESULTS

Aging Impairs Beige Adipogenesis and Promotes Fibrogenesis

Human brown fat activity levels decline with aging, correlating with a decrease in metabolic rate and increase in fat mass (Cypess et al., 2009; Ouellet et al., 2011; Pfannenberg et al., 2010; Yoneshiro et al., 2011). The development of UCP1+ beige adipocytes in response to cold or the β3 agonist CL316,243 (CL) was drastically reduced in aged (12-month-old) compared to young (2-month-old) mice (Figures 1A, 1B, and S1A–S1D), consistent with the results from other studies (Berry et al., 2017; Rogers et al., 2012). Beige fat cells in iWAT develop via the activation of thermogenic genes in mature adipocytes (i.e., beige conversion of mature adipocytes) or through the beige adipogenic differentiation of precursor cells (Berry et al., 2016; Lee et al., 2012, 2015; Shao et al., 2016; Wang et al., 2013). To determine if aging reduces the differentiation of beige adipocytes, we compared the beiging response in young and aged *AdipoChaser* mice (*Adipoq^rtTA; TRE^Cre; Rosa26R^mT/mG*) (Wang et al., 2013). Doxycycline (dox) treatment of these mice induced GFP expression in mature (PLIN1+) adipocytes (pulse) (Figures S1E and S1F). After CL treatment (chase), the iWAT of young mice contained large areas of GFP(−) (i.e., new) multilocular beige adipocytes, with the proportion of GFP(−) adipocytes increasing from ∼5% to >35% (Figures S1F and S1G). By contrast, CL treatment did not increase the proportion of unlabeled adipocytes in old mice, indicative of impaired adipogenesis (Figures S1F and S1G).

We used RNA-seq to profile iWAT gene expression in young and aged mice, treated with either vehicle or CL. iWAT from aged mice displayed a blunted upregulation of many thermogenic genes in response to CL treatment, including genes involved in oxidative phosphorylation and electron transport chain activity (Figure S1H). CL treatment also downregulated the expression of extracellular matrix (ECM) and fibrosis marker genes in young iWAT, whereas these genes were unchanged or increased in iWAT from aged animals (Figures 1C–1E and S1I). These fibrosis-signature genes (e.g., *Col1a1, Col3a1, Loxl1, Lox, Fbln2*) were expressed at higher levels in stromal-vascular cells (SVCs; a population enriched for precursor cells) than in mature adipocytes, and their expression levels in SVCs were decreased by cold exposure (Figures 1F and S1J). Finally, CL treatment decreased the expression of fibrosis genes in SVCs from young but not aged mice (Figure 1G). At a histological level, CL treatment decreased collagen deposition and fibrosis in the iWAT of young mice but augmented fibrosis in aged animals (Figure 1H). Notably, aging did not impair BAT activation or induce

(B) Relative mRNA levels of brown fat marker genes *Ucp1* and *Cidea*. n = 4 mice per group.

(C) Heatmap of gene expression profiles comparing iWAT from young and aged mice, treated with vehicle or CL.

(D) Gene ontology (GO) and pathway analysis of genes downregulated by CL selectively in young versus aged mice (red cluster, C). KG, KEGG pathway; MF, molecular function; BP, biological process; CC, cellular component.

(E) Relative mRNA levels of fibrosis marker genes in iWAT. n = 4 mice per group.

(F) Relative mRNA levels of fibrosis marker genes in stromal vascular cells (SVCs) and mature adipocytes from young mice housed at thermoneutrality or exposed to 4°C for 1 week. n = 3 mice per group.

(G) Relative mRNA levels of fibrosis marker genes in SVC from young and aged mice housed at thermoneutrality and treated with vehicle or CL for 4 days. n = 3 mice per group.

(H) Picrosirius red staining of collagen fibers in iWAT from young and aged mice treated with vehicle (Ctl) or CL. Scale bar, 50 μM.

All data are presented as mean ± SEM; *p < 0.05, **p < 0.01, ***p < 0.001 as analyzed by two-tailed Student's t test.
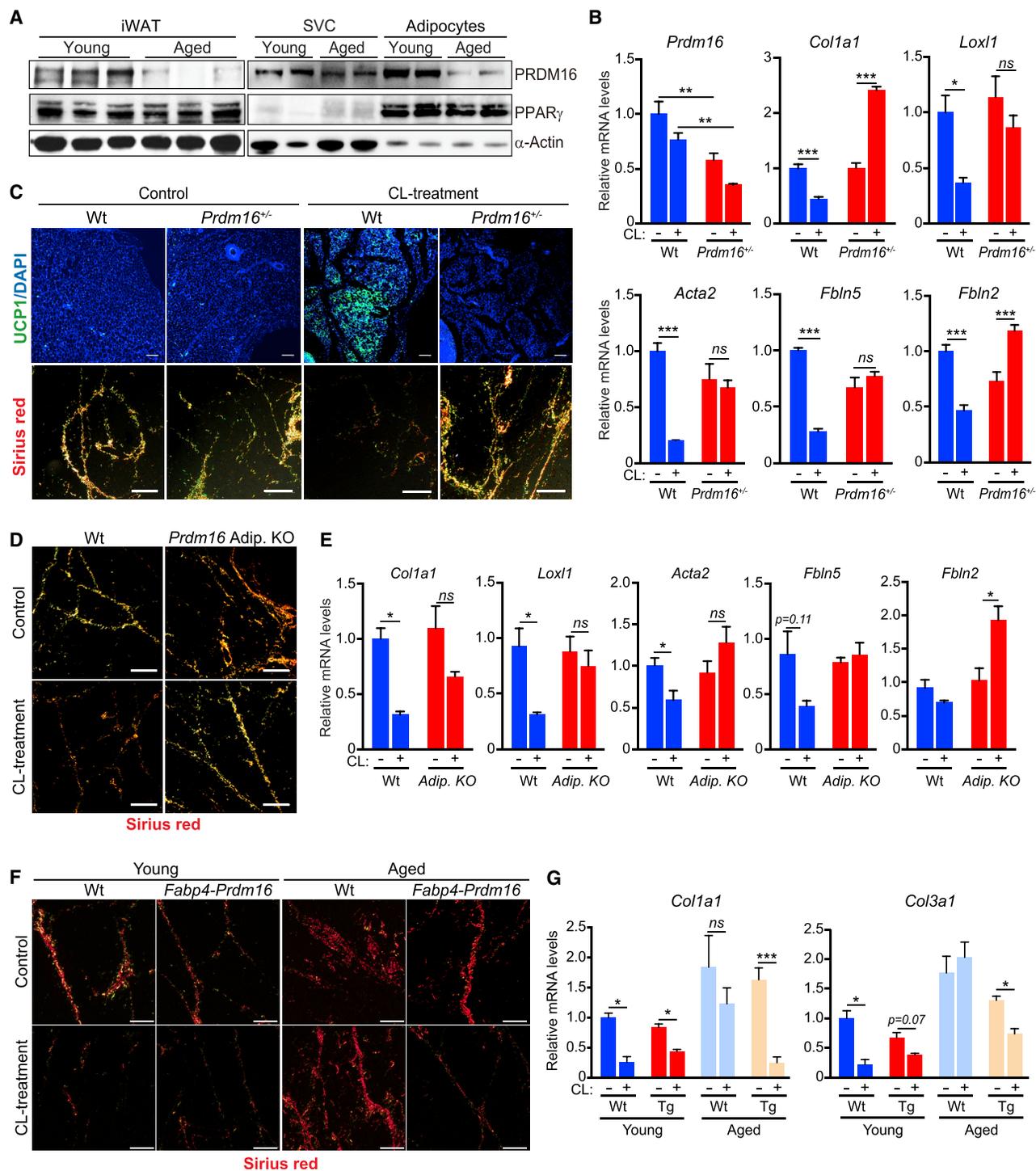
Figure 2. PRDM16 Promotes a Fibrogenic-to-Adipogenic Cell Fate Shift during WAT Beiging

(A) Western blot analysis of PRDM16, PPARγ, and α-Actin protein levels in whole iWAT (left) or in isolated adipocytes and stromal-vascular cells (SVCs) from iWAT of young and aged mice acclimated to thermoneutrality.

(B and C) Wild-type (Wt) and $Prdm16^{+/-}$ mutant mice were housed at thermoneutrality and treated with vehicle (Control) or CL for 4 days. n = 3–4 mice per group.

(B) Relative mRNA levels of $Prdm16$ and fibrosis marker genes in iWAT.

(C) UCP1 immunofluorescence (top) and Picrosirius red staining of collagen fibers (bottom) in iWAT. Scale bar, 50 μM.

(D and E) Thermoneutral-acclimated wild-type (Wt) and adipocyte-selective $Prdm16$-knockout ($Adipoq^{Cre}Prdm16$-KO) mice were treated with vehicle control or CL for 4 days. n = 3–4 mice per group.

(D) Picrosirius red staining of collagen fibers in iWAT. Scale bar, 50 μM.

(E) Relative mRNA levels of fibrosis marker genes in iWAT.

fibrotic changes in BAT (Figures S1A–S1C). Together, these findings indicate that thermogenic stimuli induce a fibrogenic-to-adipogenic phenotypic shift in iWAT stromal cells and that this process is impaired by aging.

PRDM16 Protects against Aging-Induced Adipose Fibrosis

The transcription factor PRDM16, which regulates the transcription of thermogenic genes in adipocytes, is required to maintain BAT fate during aging (Harms et al., 2014). Aging decreased PRDM16 levels in iWAT, but not in BAT of mice housed at 30°C (Figures 2A and S2A), correlating with the selective loss of beige fat developmental potential. The reduction of PRDM16 expression in iWAT was more pronounced in adipocytes than in SVC (Figure 2A).

To assess if PRDM16 regulates the fibrogenic versus adipogenic fate of precursors, we compared the beiging response in littermate wild-type and heterozygous *Prdm16*^{+/−} mutant mice. *Prdm16* expression was reduced by ~50% in the iWAT of *Prdm16*^{+/−} animals, approximating the PRDM16 reduction observed during aging (Figures 2A, 2B, and S2B). In wild-type animals, CL induced the formation of UCP1+ beige adipocytes and decreased the number and the thickness of collagen streaks (Figures 2C and S2C). By contrast, *Prdm16*^{+/−} iWAT displayed a near-complete loss of CL-induced beige fat development and retained high levels of collagen deposition (Figure 2C). Fibrosis genes that were downregulated by CL in wild-type iWAT were either unchanged or increased by CL in *Prdm16*^{+/−} iWAT (Figures 2B and S2C). The anti-fibrogenic and browning effects of CL treatment in iWAT were also decreased by adipocyte-selective *Prdm16* deficiency (*Adipoq*[Cre]) (Figures 2D, 2E, and S2D).

We next assessed whether elevating PRDM16 expression in adipocytes (of *Fabp4-Prdm16* transgenic mice) could ameliorate aging-induced fibrosis and prevent the loss of beige fat development. CL treatment decreased collagen deposition and lowered the levels of fibrosis genes (i.e., *Col1a1*, *Col3a1*) in the iWAT of 1-year-old *Prdm16*-transgenic but not control (wild-type) mice (Figures 2F, 2G, and S2E). Transgenic PRDM16 expression also facilitated the development of UCP1+ beige adipocytes in the iWAT of aged animals (Figure S2F). Given that the *Fabp4* promoter is not entirely restricted to adipocytes (Lee et al., 2013; Mullican et al., 2013; Stine et al., 2015), it is possible that PRDM16 function in another cell type contributes to the phenotype of *Fabp4-Prdm16* animals. However, the reciprocal effects of PRDM16 gain- and loss-of-function strongly suggest that PRDM16 action in adipocytes suppresses fibrogenic responses and stimulates beige fat development.

Adipocyte PRDM16 Controls Precursor Cell Fate through a Paracrine Pathway

The HIF1α and TGFβ pathways are major drivers of myofibroblast differentiation. HIF1α activation, in particular, is sufficient

to drive adipose fibrosis in the setting of obesity (Halberg et al., 2009). We found that HIF1α levels were elevated in the iWAT of aged relative to young animals (Figure S3A). Activation of HIF1α in primary iWAT precursor cells via treatment with dimethyloxaloylglycine (DMOG) induced a myofibroblast phenotype, including elevated smooth muscle actin (ACTA2) expression and the formation of actin stress fibers (Figures S3B and S3C). HIF1α activation also blocked adipocyte differentiation, including suppressing lipid accumulation and preventing the induction of adipocyte marker genes (*Pparg*, *Adipoq*) (Figures S3D and S3E). DMOG did not induce myofibroblast development or inhibit adipogenesis in *Hif1α*-deficient precursor cells, showing that the effects of DMOG were HIF1α dependent (Figures S3B–S3E).

To determine if PRDM16 interacts with HIF1α to regulate precursor cell fate, we transduced iWAT precursor cells with PRDM16-expressing or control retrovirus and used DMOG to activate HIF1α (Figure 3A). PRDM16 expression did not affect HIF1α protein levels or vice versa (Figures 3B and S3F). Under vehicle-treated (standard) conditions, PRDM16 expression did not influence adipocyte differentiation efficiency (Figures 3C and 3D). Strikingly however, PRDM16 blocked the HIF1α-mediated induction of ACTA2+ stress fibers (Figure 3C). PRDM16 also restored the adipocyte differentiation capacity of DMOG-treated cells, including promoting lipid accumulation and activating the expression of adipocyte marker genes (*Pparg*, *Fabp4*, *Ucp1*) (Figures 3C and 3D).

Surprisingly, even a low level of PRDM16-transduction efficiency (~20% of cells) prevented myofibrogenic differentiation across the culture (Figure S3G), suggesting that PRDM16 might act via a cell non-autonomous pathway. Therefore, we tested if conditioned medium (CM) from PRDM16- or GFP-expressing (control) adipocytes could modulate precursor differentiation (Figure 3E). CM from PRDM16-expressing adipocytes (P-CM) recapitulated the effect of PRDM16 expression in suppressing HIF1α-induced stress-fiber formation, whereas CM from GFP-expressing cells (GFP-CM) had a more limited effect (Figures 3F and 3G). Moreover, P-CM stimulated beige adipocyte differentiation in HIF1α-expressing cells, including promoting lipid droplet formation and inducing the expression of adipocyte genes (*Pparg*, *Adipoq*, *Ucp1*) (Figures 3H, 3I, and S3H). P-CM also suppressed the pro-fibrogenic and anti-adipogenic effects of TGFβ treatment (Figures 3J, 3K, and S3I). These results indicate that P-CM represses a common downstream step in the myofibrogenic program and enhances the adipogenic commitment of precursor cells.

To test whether PRDM16 is required for the production of adipogenic paracrine signal(s) by adipocytes, we compared the activity of CM from control (wild-type) and *Prdm16* knockout (KO) adipocytes from iWAT (Figure S3J). For these assays, we used a lower dose of DMOG to achieve modest elevation of HIF1α, which nonetheless blocked adipocyte differentiation (Figure S3K). Treatment of these cultures with CM from control adipocytes

(F and G) young (2-month-old) and aged (12-month-old) wild-type (Wt) and *Fabp4-Prdm16* mice were acclimated to thermoneutrality and treated with CL for 4 days. n = 3–5 mice per group.
(F) Picrosirius red staining of collagen fibers. Scale bar, 50 μM.
(G) Relative mRNA levels of fibrosis marker genes in iWAT.
All data are presented as mean ± SEM; *p < 0.05, **p < 0.01, ***p < 0.001 as analyzed by two-tailed Student's t test.
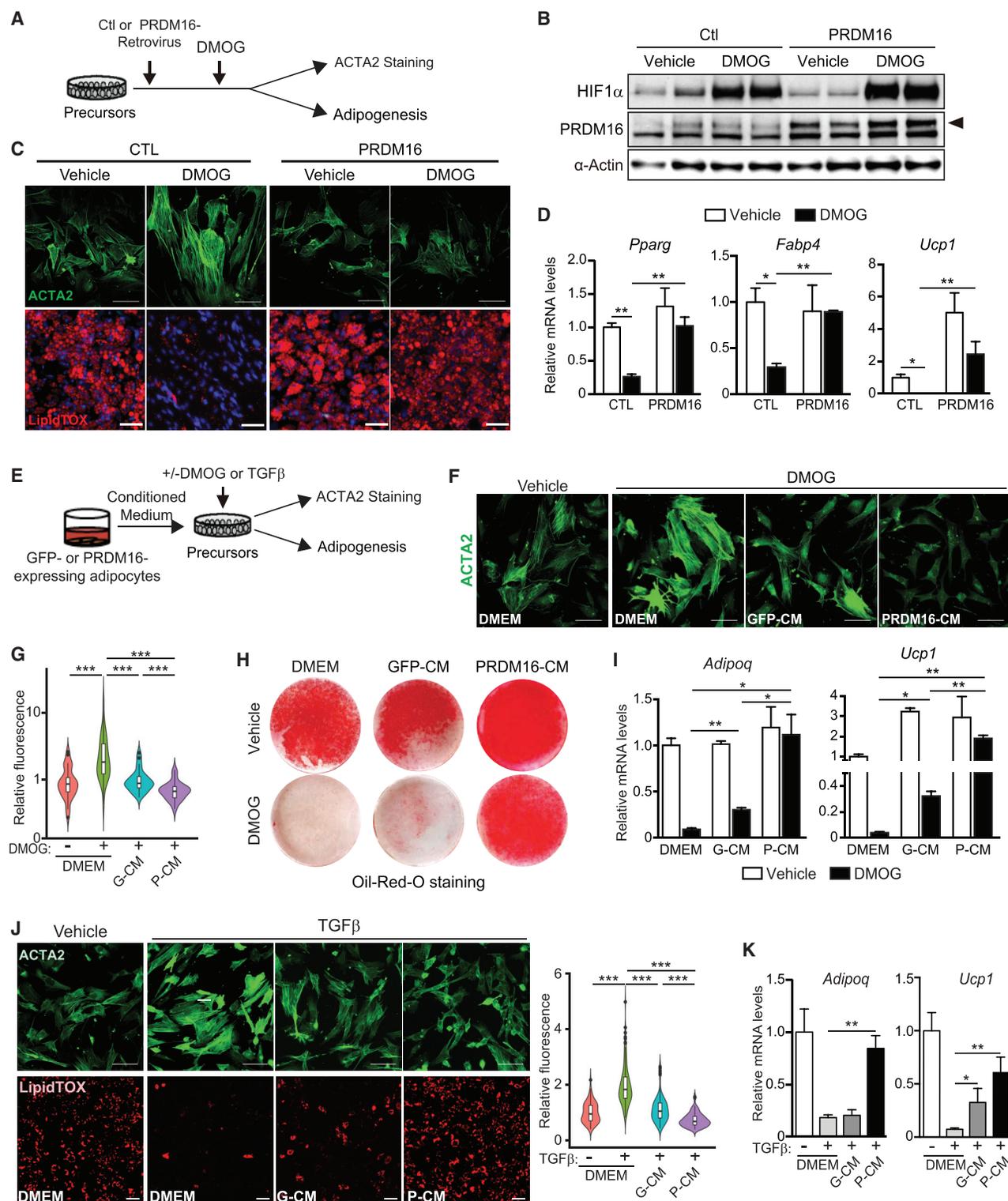
Figure 3. Adipocyte PRDM16 Controls Precursor Fate through a Paracrine Pathway

(A–D) iWAT precursor cells were transduced with control (CTL) or PRDM16-expressing retrovirus and treated with either vehicle control (CTL) or DMOG. After 2 days, cells were immunostained for ACTA2 or induced to differentiate into adipocytes for 5 days.

(A) Experimental schema.

(B) Western blot analysis of HIF1α, PRDM16, and α-Actin protein levels.

(C) ACTA2 immunostaining (green) (top panel) and LipidTOX staining (red) of lipid droplets in differentiated adipocytes (bottom panel). Scale bar, 100 μM (top); 200 μM (bottom).

improved adipocyte differentiation, while CM from *Prdm16* KO cells had minimal activity (Figures S3K and S3L). Collectively, these data demonstrate that PRDM16 promotes the secretion of a paracrine factor(s) that can suppress myofibrogenesis and stimulate adipogenic competency in precursor cells.

PRDM16-Driven FAO Is Required for the Production of Paracrine Effectors

The adipogenic activity of P-CM was decreased by charcoal treatment but resistant to heating, suggesting that the active component could be a water-soluble metabolite (Figure S4A). RNA-seq and gene ontology analysis identified "fatty acid tria-cylglycerol and ketone body metabolism" as enriched pathways in PRDM16-expressing versus control adipocytes (Figure 4A). PRDM16 expression increased the levels of many fatty acid oxidation (FAO) and ketone metabolism genes (e.g., *Cpt1*, *Cpt2*, *Acadl*, *Acadm*, *Hmgcs2*) in adipose cells (Figures 4B and S4B). In particular, PRDM16-expressing cells expressed 10-fold higher levels of *Cpt1b* (Figure S4B), which encodes the rate-limiting enzyme in FAO. Moreover, transgenic expression of PRDM16 in iWAT adipocytes increased FAO gene levels and CPT1b protein levels (Figures S4C and S4D). Reciprocally, ag-ing-induced or genetic loss of PRDM16 in iWAT or isolated adipocyte cultures decreased FAO gene levels and CPT1b protein levels (Figures S4E–S4H). At a functional level, PRDM16-ex-pressing cells generated >20-fold higher levels of acetyl-coA from 13C-labeled palmitate than did control cells, indicating much higher rates of FAO (Figures 4C and S4I). Finally, metabo-lomic analyses revealed increased levels of tricarboxylic acid (TCA) cycle intermediates and reduced levels of glycolytic me-tabolites in PRDM16-expressing adipocytes (Figure 4D).

To determine whether FAO was necessary for the paracrine ac-tivity of PRDM16-expressing adipocytes, we treated PRDM16-expressing cells with the CPT1 inhibitor, etomoxir (Eto), or vehicle (control) for 24 h prior to collecting CM (Figure 4E). Eto treatment blocked FAO in adipocytes, as assayed by ^{3}H-palmitate oxidation (Figure S5A). The CM from Eto-treated adipocytes had a severely diminished capacity to promote adipogenesis and adipocyte gene expression in HIF1α-express-ing cells (Figures 4F and 4G). Treatment of precursor cultures directly with Eto resulted in a mild impairment of adipocyte differentiation.

We further investigated whether acute inhibition of FAO in mice disrupts CL-induced beige fat remodeling. Mice housed at thermoneutrality were treated with CL to induce beiging along with either vehicle or Eto (Figure S5B). Eto treatment blocked the induction of UCP1+ beige adipocytes and decreased the expression levels of thermogenic genes, including a 90% reduc-tion in *Ucp1* levels (Figures S5C and S5D). We used *AdipoChaser* reporter mice (Wang et al., 2013) to determine whether FAO is required for adipogenesis (Figures 4H and 4I). Doxycycline administration in these mice induced the expression of mGFP in adipocytes (pulse). This was followed by a chase period, during which mice were treated with CL to induce beiging along with either vehicle or Eto for 5 days. iWAT from control mice (CL + vehicle) underwent beige adipogenesis, as evidenced by the development of GFP-negative multilocular adipocytes (induced from ∼5% to 25%; Figure 4I, middle-bottom panel; red PLIN+ adipocytes without GFP). By contrast, GFP-negative adipocytes remained at background levels in the iWAT of Eto-treated mice (Figure 4I, bottom-right panel; yellow = red PLIN+ colocalized with green GFP+). In addition to blocking beige adipogenesis, Eto prevented the beiging of mature adipocytes. Furthermore, Eto treatment induced the appearance of fibrotic streaks and augmented the expression of fibrosis genes (Figures S5C and S5D). These findings suggest that PRDM16-driven FAO is required for the production of a paracrine factor(s) that affects precursor differentiation.

PRDM16 Drives the Production and Export of β-Hydroxybutyrate (BHB)

The ketone body β-hydroxybutyrate (BHB) is a small polar metabolite that has signaling functions in a variety of biological contexts (Newman and Verdin, 2014). We noted that PRDM16 regulates the expression of the rate-limiting ketogenic enzyme *Hmgcs2* (Figures 4B, S4B, and S4C). LC-MS analysis of metabolites identified a striking ∼10-fold increase of BHB levels in P16-CM (∼200 μM) compared to that in GFP-CM (∼20 μM) (Figure 5A). The concentration of BHB in CM increased in a time-dependent manner, indicative of an active process (Fig-ure 5B). The ketogenic precursor 3-hydroxy-3-methylglutaryl-Coenzyme A (HMG-CoA) also accumulated over the same period (Figure 5C). The secretion rate of BHB in PRDM16-ex-pressing cells was ∼12 nmol/mg protein/min, 6-fold higher than that in control adipocytes (Figure 5D). Metabolic tracing showed elevated incorporation of ^{13}C from ^{13}C-palmitate into BHB in PRDM16-expressing versus control adipocytes, sug-gesting that adipocyte FAO-flux fuels BHB production (Fig-ure 5E). Notably, BHB levels increased in iWAT by 1 day of cold exposure and remained elevated at 7 days (Figure 5F).

(D) Relative mRNA levels of adipocyte genes. n = 3 per group.

(E–K) iWAT precursor cells were treated with: (1) control medium (DMEM), conditioned medium (CM) from GFP-expressing adipocytes (GFP-CM), or CM from PRDM16-expressing adipocytes (P-CM); and (2) vehicle, DMOG or recombinant TGFβ. After 24 h, cultures were immunostained for ACTA2 or induced to differentiate into adipocytes for 5 days.

(E) Experimental schema.

(F) ACTA2 immunostaining (green). Scale bar, 100 μm.

(G) Violin plots show relative fluorescent intensity per cell in indicated groups (from F). The white solid boxes represent percentiles (bottom of box = 25th, horizontal line = 50th, top of box = 75th). n = 50–80 cells per condition.

(H) Oil-Red-O staining (red) of adipocyte lipid droplets.

(I) Relative mRNA levels of adipocyte genes in cultures from (H). n = 3–5 per group.

(J) ACTA2 immunostaining (top; green) and LipidTOX staining (bottom; red) of lipid droplets in cultures treated with indicated CM and either vehicle or TGFβ. Scale bar, 100 μm. Violin plots show relative ACTA2 fluorescent intensity per cell (right).

(K) Relative mRNA levels of adipocyte marker genes in cultures from (J, bottom). n = 3–5 per group.

All data are presented as mean ± SEM Analysis by two-way ANOVA with Tukey correction.

A Genes upregulated in PRDM16-expressing cells

B FAO & Ketone metabolism

C FAO

D

E

F

G *Pparg* *Adipoq*

H *Apn-rtTA; TRE-Cre; Rosa26^mGFP*

I
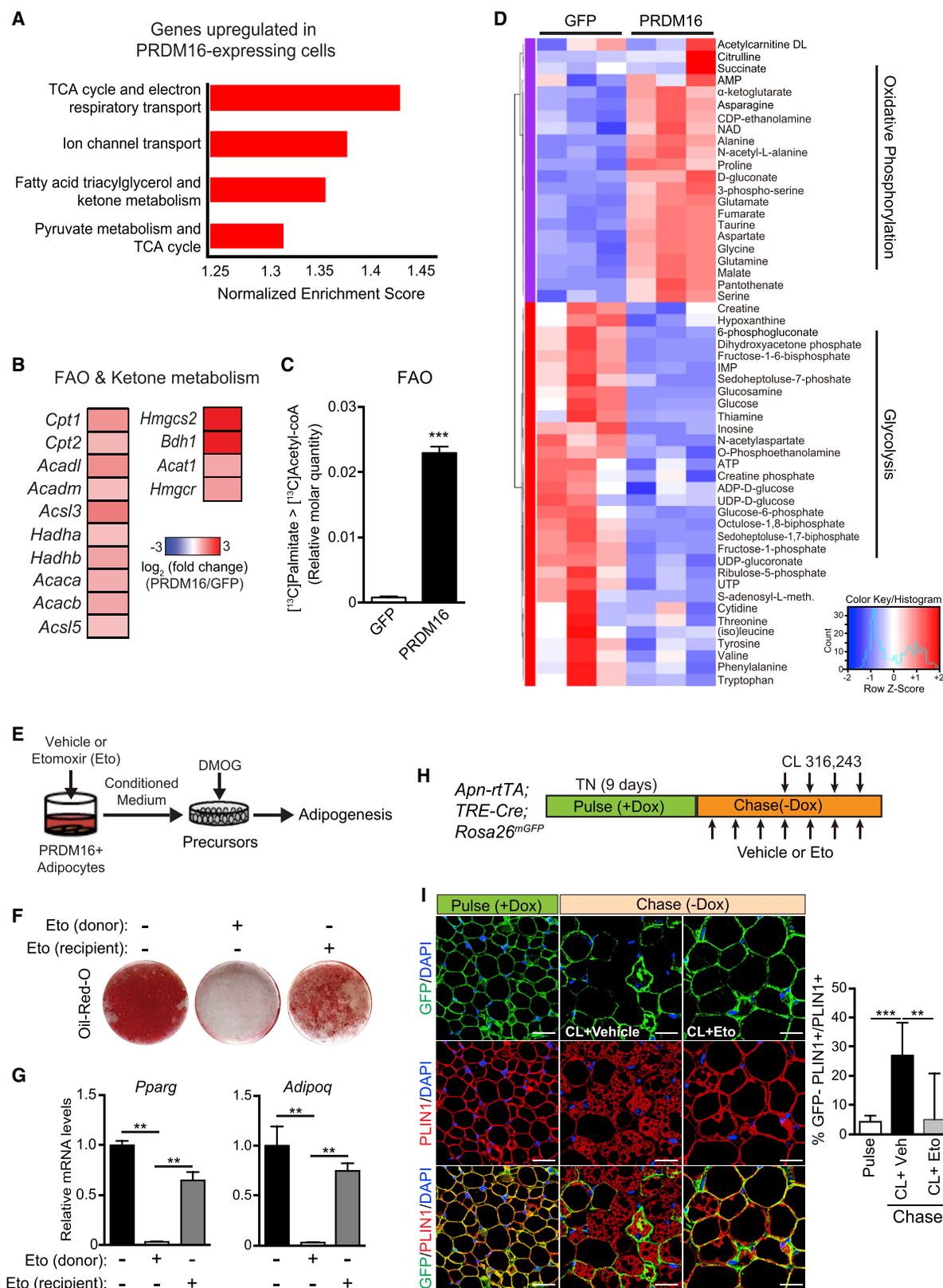
Figure 4. PRDM16-Driven FAO Is Required for the Production of Paracrine Effectors

(A) Gene set enrichment analysis (GSEA) of genes upregulated in PRDM16-expressing versus control cells. Enriched pathways were defined by a normalized enrichment score >1.3 and FDR <0.05.

(legend continued on next page)

This cold-induced increase in iWAT BHB levels was diminished in *Prdm16*^{+/−} animals (Figure 5G). Additionally, the cold-stimulated rise in iWAT tissue BHB levels was absent in aged mice, though serum BHB levels rose to a similar degree in young and aged animals (Figure S5E). Finally, CL treatment increased BHB levels in BAT and iWAT (Figure S5F). These data suggest that BHB is produced locally or selectively accumulates in the iWAT of young animals.

BHB Inhibits Myofibrogenesis and Enhances Beige Adipogenesis

We next examined whether BHB could modulate the differentiation activity of precursor cells (Figure 5H). Exposure of cells to BHB mimicked the effect of P-CM in diminishing the formation of ACTA2+ stress fibers upon HIF1α activation or TGFβ treatment (Figures 5I and 5J). BHB also rescued the adipocyte differentiation potential of HIF1α-expressing or TGFβ-treated precursors (Figure 5K). Similar adipogenic effects of BHB were observed in primary human subcutaneous adipose-derived stem cells (hASCs) (Figures S5G and S5H).

BHB is catabolized by cells to generate intermediary metabolites, including acetyl-coA. Additionally, BHB can have a variety of signaling functions, including inhibiting class 1 histone deacetylases and acting as a ligand for certain G-protein coupled receptors (Newman and Verdin, 2014). To determine if the metabolism of BHB is required for its effects in adipose precursors, we used lentiviral shRNA constructs to reduce the expression of 3-Hydroxybutyrate Dehydrogenase 1 (BDH1), which catalyzes the first step in BHB catabolism (Figure 6A). Depletion of *Bdh1* modestly decreased the adipogenic conversion of precursor cells and *Pparg* expression under basal conditions (Figures 6B and 6C). However, *Bdh1* depletion ablated the capacity for BHB to restore adipocyte differentiation capacity in HIF1α-expressing cells (Figures 6B and 6C).

We next sought to determine whether BDH1 activity in precursor cells is required for beige adipocyte development *in vivo*. To do this, we generated a mouse model for inducible deletion of *Bdh1* in *Pdgfrα+* precursor cells. Incorporation of a tdTomato reporter gene allowed us to track the developmental fates of wild-type and *Bdh1* null precursors (*Bdh1*[P-KO]). We treated thermoneutral-housed adult mice with tamoxifen to induce tdTomato expression and concurrently delete *Bdh1* in *Pdgfrα+* cells (of *Bdh1*[P-KO] animals) (Figure 6D). Flow cytometry analysis immediately after tamoxifen treatment (pulse) showed that a similar proportion of PDGFRα+ cells were marked by tdTomato expression in control (wild-type) and *Bdh1*[P-KO] animals and that *Bdh1* levels were decreased in PDGFRα+ cells from the mutant mice (Figures 6E and S6A). Immunofluorescence staining shows that tdTomato expression was specifically activated in PDGFRα+ cells (Figure S6B). Mice were also exposed to 4°C to stimulate beige fat development. In control mice, nearly 40% of tdTomato+ cells contributed to the development of new PLIN1+ lipid-containing adipocytes (Figures 6F and 6G). By contrast, there was minimal conversion of *Bdh1*-deleted cells into mature adipocytes, with most tdTomato+ cells remaining PLIN1 negative (Figures 6F and 6G). At this time point, the expression of several fibrosis genes trended toward higher expression in mutant iWAT (Figure S6C). These results reveal an essential role for BHB metabolism in facilitating the differentiation of adipose precursor cells.

Lastly, we investigated whether raising BHB levels in aged animals could induce beige fat development and ameliorate fibrosis. To do this, we fed 1-year-old mice a diet containing the ketone ester (KE) (R)-3-hydroxybutyl (R)-3-hydroxybutyrate. This KE is hydrolyzed in the small intestine to generate BHB and 1,3-butanediol, which is further metabolized by the liver into BHB and acetoacetate (Figure 7A). Animals were pair fed KE diet or a calorie-matched control diet for 30 days, concluding with 4 days of cold exposure to induce beiging (Figure 7B). KE feeding raised plasma BHB levels by 10-fold compared to that in control fed mice (3–4 mM compared to 0.4 mM; Figure 7C). Body weights were the same between mice on the KE and control diets (Figure 7D), while the KE-fed mice had significantly lower blood glucose levels (Figure 7E).

Histological assessments show that iWAT of control mice contained mostly large unilocular white-like adipocytes, whereas the iWAT of KE mice developed multilocular beige-like adipocytes in (Figure 7F). There was also a prominent decrease in the number and size of fibrotic streaks in the iWAT of KE-fed mice (Figure 7F). At the molecular level, the iWAT from KE mice expressed elevated levels of brown fat-marker genes, including a 7-fold increase in *Ucp1* and lower levels of fibrosis marker genes (e.g., *Col1a1*, *Col3a1*, *Acta2* and *Lox*) (Figure 7G). KE feeding was not sufficient to reduce fibrosis or promote beige fat development in the absence of cold exposure (Figures S7A and S7B). These results demonstrate that BHB treatment can restore beige adipocyte developmental competency in old animals.

(B) Expression heatmap of "fatty acid oxidation (FAO) and ketone body metabolism" genes in PRDM16-expressing versus control cells.

(C) Quantification of FAO. Adipocytes were cultured in medium containing U-^{13}C-palmitate for 6 h prior to metabolite analysis by LC-MS. Relative molar quantity of [13]C_2-labeled acetyl-CoA in GFP- and PRDM16-expressing adipocytes was calculated by multiplying % molar enrichment of [13]C_2-labeled acetyl-CoA by relative total acetyl-CoA quantitation. n = 3–4 per group.

(D) Heatmap showing standardized amounts of indicated metabolites in GFP- and PRDM16-expressing adipocytes, across samples (*Z* score). n = 3 per group.

(E–G) PRDM16-expressing adipocytes (donor) were treated with vehicle or Etomoxir (Eto) for 24 h prior to collecting conditioned medium (CM). HIF1α-expressing (DMOG-treated) precursors were treated with CM and induced to undergo adipocyte differentiation. To control for effects of Eto carried over in CM, a subset of recipient cells was directly exposed to Eto [Eto(recipient)] by mixing Eto with P-CM prior to treatment.

(E) Experimental schema.

(F) Oil-Red-O staining of cultures after adipogenic induction.

(G) Relative mRNA levels of adipocyte genes in cultures from (F). n = 4–5 per group.

(H and I) *AdipoChaser* (*Adipoq*[rtTA];*TRE*[Cre];*Rosa26*[mTmG]) mice were pulse labeled by feeding them with doxycyxline (dox) chow (600 mg/kg) for 9 days. During the 3-day washout period, mice were treated with Eto or vehicle for 3 days, followed by treatment with CL and either Eto or vehicle for another 4 days (chase).

(I) Immunofluorescence staining of PLIN1 (red) in adipocytes and GFP reporter (green). Quantification of adipogenesis (% GFP[−]/total PLIN1+ cells) (right).

All data are presented as mean ± SEM; *p < 0.05, **p < 0.01, ***p < 0.001 as analyzed by two-tailed Student's t test.
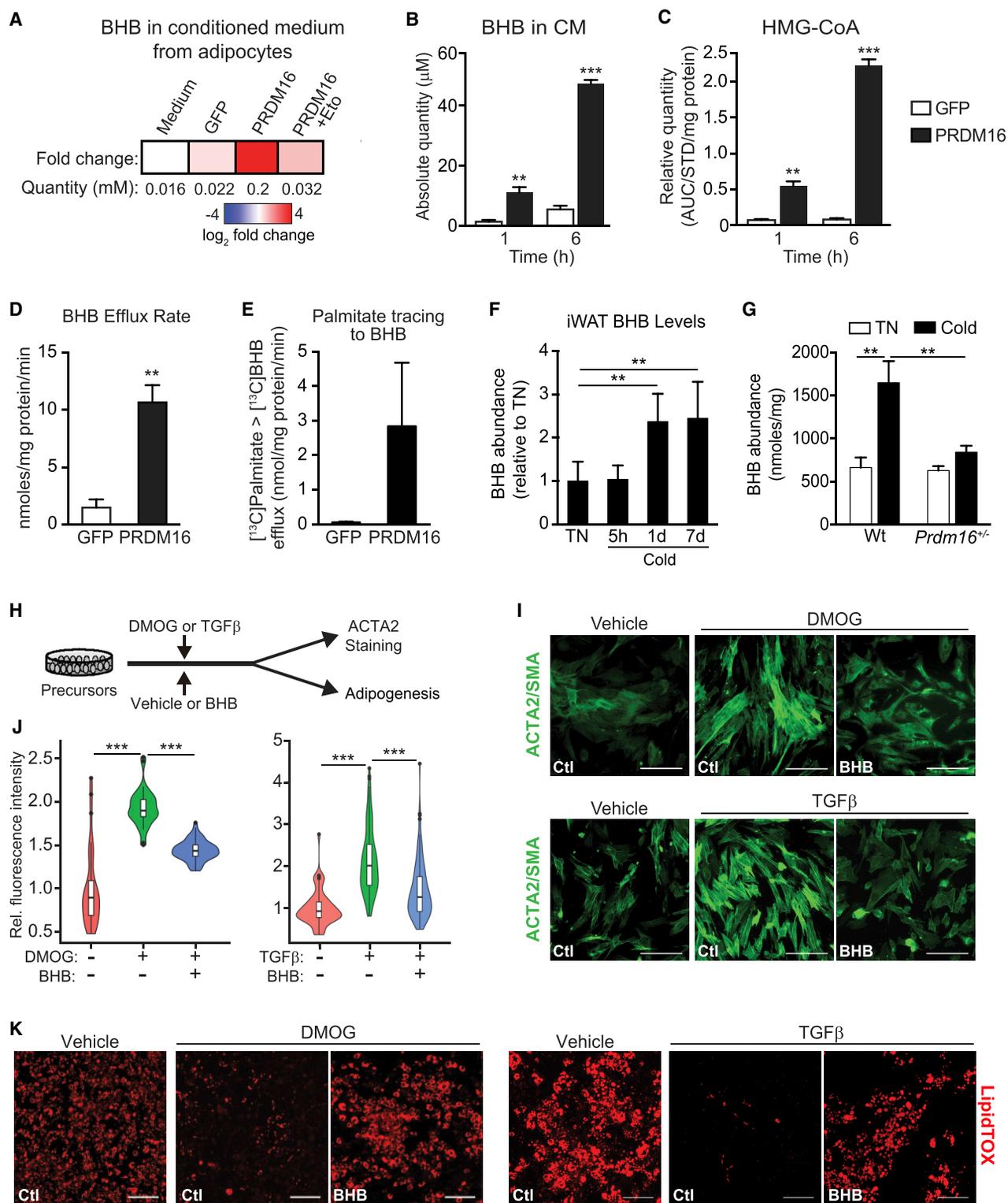
Figure 5. PRDM16 Drives the Production of β-Hydroxybutyrate (BHB), which Suppresses Fibrogenesis

(A) BHB concentration in conditioned medium from control (GFP) and PRDM16-expressing adipocytes in the presence or absence of Eto treatment, as determined by LC-MS.

(B) Absolute quantity of BHB in GFP-CM and P-CM collected at 1 h and 6 h time points. n = 4 per group.

(C) Relative quantity of HMG-CoA in GFP- and PRDM16-expressing adipocytes at 1 h and 6 h time points. AUC, area under the curve. AUC for HMG-CoA was normalized to $^{13}C_3^{15}N_1$-HMG-CoA internal standard (STD) and total protein in each sample. n = 4 per group.

Figure 6. BHB Catabolism Regulates Adipose Precursor Differentiation

(A–C) iWAT precursor cells were transduced with scramble (shScr) or *Bdh1* shRNA lentivirus and treated with vehicle, DMOG alone, or DMOG plus BHB. After 2 days, cells were induced to differentiate into adipocytes for 5 days.

(A) Relative mRNA levels of *Bdh1* in iWAT precursor cells. n = 4 per group.

(B) Oil-Red-O staining (red) of lipid droplets in differentiated adipocytes.

(C) Relative mRNA levels of adipogenic genes in differentiated cultures. n = 4 per group.

(D–G) *Bdh1* KO (*Pdgfra^CreERT2^; Bdh1^flox/flox^; R26R^tdTomato^*) and matched control (ctrl; *Pdgfra^CreERT2^; Bdh1^+/+^; R26R^tdTomato^* or *Pdgfra^CreERT2^; Bdh1^flox/+^; R26R^tdTomato^*) mice were treated with tamoxifen for 4 days. iWAT was analyzed from mice at day 0 (pulse) and following 2-week cold exposure (day 23).

(D) Experimental schema.

(E) Flow cytometry analysis showing proportion of PDGFRα+ cells expressing tdTomato in ctrl and *Bdh1 KO* iWAT (left). Relative mRNA levels of *Bdh1* in tdTomato+; PDGFRα+ cells from ctrl and *Bdh1 KO* iWAT (right). n = 3 mice per group.

(F) Immunofluorescence staining of tdTomato (red) and PLIN1 (green) in iWAT. Scale bar, 200 μM.

(G) Quantification of adipogenesis (% tdTomato+; PLIN1+/total tdTomato+ cells). n = 30 randomly chosen 20× magnification fields from 3 mice per group. All data are presented as mean ± SEM; *p < 0.05, **p < 0.01, ***p < 0.001 as analyzed by two-tailed Student's t test.
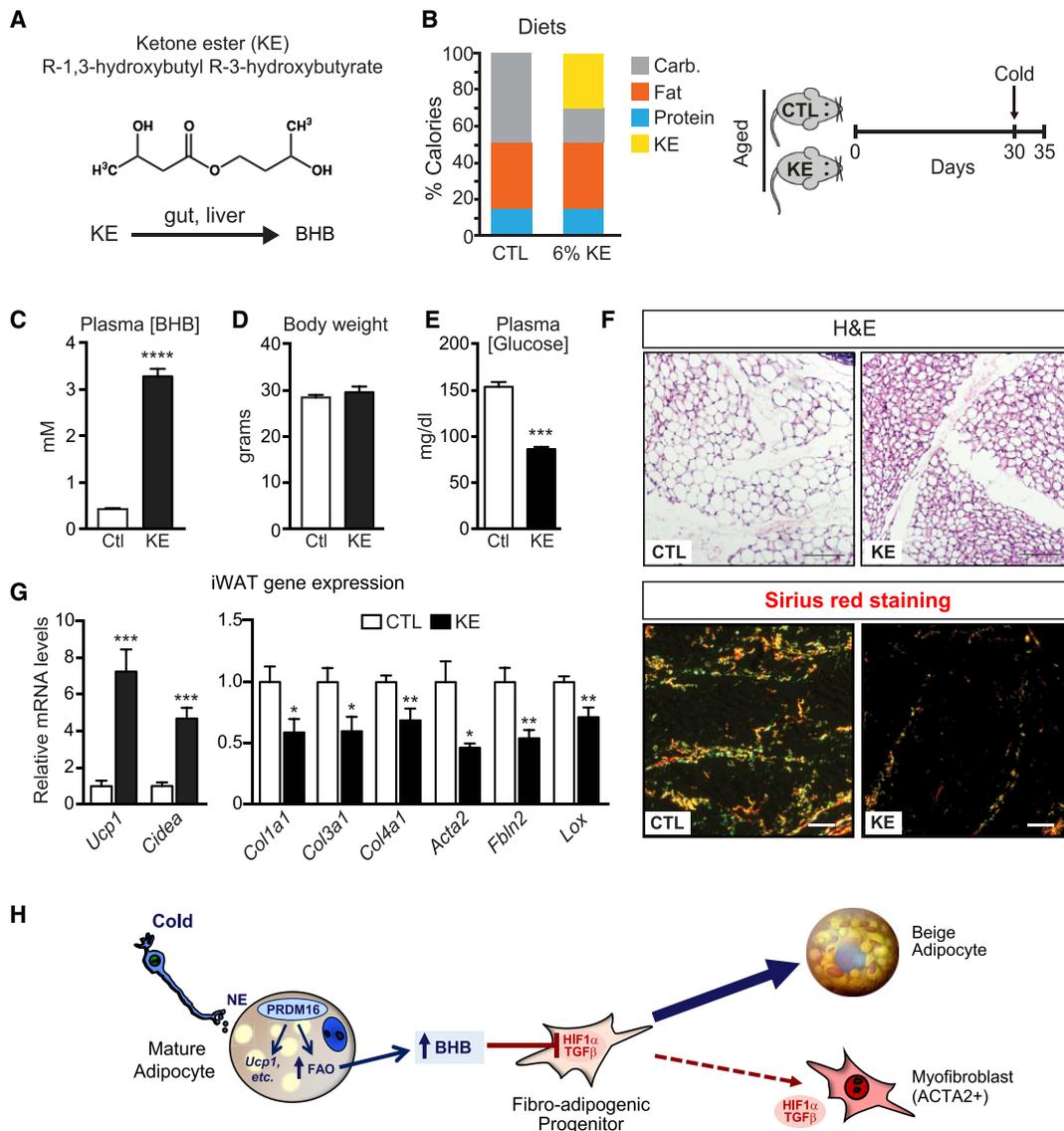
Figure 7. Raising BHB Levels in Aged Mice Alleviates Adipose Fibrosis and Restores Beige Adipogenic Potential

(A) Metabolism of the ketone ester (R-1,3-hydroxybutyl R-3-hydroxybutyrate) (KE) in the gut and liver to form BHB.

(B) Composition of control (CTL) and 6% KE diet (left) and schema of experiment (right). Aged (12-month-old) mice were fed with CTL or KE diet for 1 month at room temperature and then switched to 4°C cold for 4 days.

(C–E) Plasma BHB levels (C), body weight (D), and plasma glucose levels (E) of experimental mice. n = 10 for control diet group; n = 8 for KE diet group.

(F) Hematoxylin & Eosin (H&E) staining (top) and Picrosirius red staining (bottom) of iWAT from mice described above (B). Scale bar, 50 μM.

(G) Relative mRNA levels of thermogenic and fibrosis genes in iWAT.

All data are presented as mean ± SEM; *$p < 0.05$, **$p < 0.01$, ***$p < 0.001$ as analyzed by two-tailed Student's t test.

restored beige fat developmental potential. This suggests that even a short exposure to BHB is sufficient to rejuvenate the adipogenic differentiation competency of aged precursors.

In summary, our findings establish the existence of a metabolite-based paracrine signaling axis in beige adipose tissue, with beige adipocytes providing metabolite cues to regulate adipose precursor cell differentiation. This raises the possibility that increasing ketone metabolism in adipose tissue could ameliorate fibrosis and encourage beige fat development for combating metabolic disease.

Limitations of Study

Emerging studies indicate that adipose precursor cells, marked by their expression of PDGFRα, represent a heterogeneous cell compartment, comprising different cell types, including several putative fibrogenic populations (Burl et al., 2018; Hepler et al., 2018; Marcelin et al., 2017; Merrick et al., 2019; Schwalie et al., 2018). Future studies will determine if BHB acts preferentially on specific subpopulations of stromal cells in adipose. Additionally, our studies focused on the beiging of subcutaneous inguinal adipose tissue of mice. However, BHB appears to act

primarily via facilitating the general program of adipogenesis, common to all adipocytes. This raises the possibility that BHB could regulate white adipocyte differentiation, such as during high-fat diet feeding. It also remains uncertain whether acetoacetate, acetate, or certain short chain fatty acids could play similar roles to BHB in modulating adipose tissue remodeling responses. Finally, it is unknown whether ketone ester feeding or other ways to increase adipose BHB levels would have anti-fibrotic and/or pro-adipogenic effects in human adipose tissue.

STAR★METHODS

Detailed methods are provided in the online version of this paper and include the following:

- KEY RESOURCES TABLE
- CONTACT FOR REAGENT AND RESOURCE SHARING
- EXPERIMENTAL MODEL AND SUBJECT DETAILS
  - Mice
  - Cell Culture
- METHOD DETAILS
  - ACTA2/SMA Staining and Morphological Analysis in Cultured Cells
  - Mass Spectrometry-Based SCFA Measurements
  - SCFA Extraction from Frozen Tissues
  - *In Vitro* Isotopic Labeling
  - Water-Soluble Metabolite Extraction
  - Acyl-CoA Extraction and Measurement
  - Flow Cytometry
  - Ketone Ester (KE) Feeding
  - Fatty Acid Oxidation Assay
  - RNA-seq and Analysis
  - Histology
  - QPCR and Western Blot
- QUANTIFICATION AND STATISTICAL ANALYSIS
- DATA AND SOFTWARE AVAILABILITY

SUPPLEMENTAL INFORMATION

Supplemental Information can be found online at https://doi.org/10.1016/j.cmet.2019.05.005.

AUTHOR CONTRIBUTIONS

W.W., J.I., and P.S. were responsible for conceptualization, data analysis, and writing/review. W.W. conducted the majority of the experiments. S.T., M.T.D., and N.W.S. performed mass spectrometry analysis of metabolite levels in medium and tissues. M.S. and R.K.G. performed adipocyte fate mapping experiments. A.J.C. and J.D.R. performed metabolomic analyses. A.S. conducted microscopy analysis. H.L. performed bioinformatics analyses. S.O. and P.C. provided samples from adipocyte-selective *Prdm16*-deficient mice. J.A.B. assisted with mouse aging experiments. M.T.K. and R.L.V. provided ketone ester and detailed procedures for ketone ester feeding.

DECLARATION OF INTERESTS

The authors declare no competing interests.

REFERENCES

Adijanto, J., Du, J., Moffat, C., Seifert, E.L., Hurle, J.B., and Philp, N.J. (2014). The retinal pigment epithelium utilizes fatty acids for ketogenesis. J. Biol. Chem. *289*, 20570–20582.

Auestad, N., Korsak, R.A., Morrow, J.W., and Edmond, J. (1991). Fatty acid oxidation and ketogenesis by astrocytes in primary culture. J. Neurochem. *56*, 1376–1386.

Bernard, K., Logsdon, N.J., Ravi, S., Xie, N., Persons, B.P., Rangarajan, S., Zmijewski, J.W., Mitra, K., Liu, G., Darley-Usmar, V.M., et al. (2015). Metabolic reprogramming is required for myofibroblast contractility and differentiation. J. Biol. Chem. *290*, 25427–25438.

Berry, D.C., Jiang, Y., and Graff, J.M. (2016). Mouse strains to study cold-inducible beige progenitors and beige adipocyte formation and function. Nat. Commun. *7*, 10184.

Berry, D.C., Jiang, Y., Arpke, R.W., Close, E.L., Uchida, A., Reading, D., Berglund, E.D., Kyba, M., and Graff, J.M. (2017). Cellular aging contributes to failure of cold-induced beige adipocyte formation in old mice and humans. Cell Metab. *25*, 166–181.

Blázquez, C., Sánchez, C., Velasco, G., and Guzmán, M. (1998). Role of carnitine palmitoyltransferase I in the control of ketogenesis in primary cultures of rat astrocytes. J. Neurochem. *71*, 1597–1606.

Burl, R.B., Ramseyer, V.D., Rondini, E.A., Pique-Regi, R., Lee, Y.H., and Granneman, J.G. (2018). Deconstructing adipogenesis induced by beta3-adrenergic receptor activation with single-cell expression profiling. Cell Metab. *28*, 300–309.e4.

Cannon, B., and Nedergaard, J. (2004). Brown adipose tissue: function and physiological significance. Physiol. Rev. *84*, 277–359.

Carthy, J.M. (2018). TGFβ signaling and the control of myofibroblast differentiation: implications for chronic inflammatory disorders. J. Cell. Physiol. *233*, 98–106.

Cohen, P., Levy, J.D., Zhang, Y., Frontini, A., Kolodin, D.P., Svensson, K.J., Lo, J.C., Zeng, X., Ye, L., Khandekar, M.J., et al. (2014). Ablation of PRDM16 and beige adipose causes metabolic dysfunction and a subcutaneous to visceral fat switch. Cell *156*, 304–316.

Cypess, A.M., Lehman, S., Williams, G., Tal, I., Rodman, D., Goldfine, A.B., Kuo, F.C., Palmer, E.L., Tseng, Y.H., Doria, A., et al. (2009). Identification and importance of brown adipose tissue in adult humans. N. Engl. J. Med. *360*, 1509–1517.

Ding, H., Jiang, L., Xu, J., Bai, F., Zhou, Y., Yuan, Q., Luo, J., Zen, K., and Yang, J. (2017). Inhibiting aerobic glycolysis suppresses renal interstitial fibroblast activation and renal fibrosis. Am. J. Physiol. Renal. Physiol. *313*, F561–F565.

Douris, N., Desai, B.N., Fisher, F.M., Cisu, T., Fowler, A.J., Zarebidaki, E., Nguyen, N.L.T., Morgan, D.A., Bartness, T.J., Rahmouni, K., et al. (2017). Beta-adrenergic receptors are critical for weight loss but not for other metabolic adaptations to the consumption of a ketogenic diet in male mice. Mol. Metab. *6*, 854–862.

Fedorenko, A., Lishko, P.V., and Kirichok, Y. (2012). Mechanism of fatty-acid-dependent UCP1 uncoupling in brown fat mitochondria. Cell *151*, 400–413.

Frey, A.J., Feldman, D.R., Trefely, S., Worth, A.J., Basu, S.S., and Snyder, N.W. (2016). LC-quadrupole/Orbitrap high-resolution mass spectrometry

enables stable isotope-resolved simultaneous quantification and ^{13}C-isotopic labeling of acyl-coenzyme A thioesters. Anal. Bioanal. Chem. *408*, 3651–3658.

Halberg, N., Khan, T., Trujillo, M.E., Wernstedt-Asterholm, I., Attie, A.D., Sherwani, S., Wang, Z.V., Landskroner-Eiger, S., Dineen, S., Magalang, U.J., et al. (2009). Hypoxia-inducible factor 1alpha induces fibrosis and insulin resistance in white adipose tissue. Mol. Cell. Biol. *29*, 4467–4483.

Harms, M., and Seale, P. (2013). Brown and beige fat: development, function and therapeutic potential. Nat. Med. *19*, 1252–1263.

Harms, M.J., Ishibashi, J., Wang, W., Lim, H.W., Goyama, S., Sato, T., Kurokawa, M., Won, K.J., and Seale, P. (2014). Prdm16 is required for the maintenance of brown adipocyte identity and function in adult mice. Cell Metab. *19*, 593–604.

Harms, M.J., Lim, H.W., Ho, Y., Shapira, S.N., Ishibashi, J., Rajakumari, S., Steger, D.J., Lazar, M.A., Won, K.J., and Seale, P. (2015). PRDM16 binds MED1 and controls chromatin architecture to determine a brown fat transcriptional program. Genes Dev. *29*, 298–307.

Hasegawa, Y., Ikeda, K., Chen, Y., Alba, D.L., Stifler, D., Shinoda, K., Hosono, T., Maretich, P., Yang, Y., Ishigaki, Y., et al. (2018). Repression of adipose tissue fibrosis through a PRDM16-GTF2IRD1 complex improves systemic glucose homeostasis. Cell Metab. *27*, 180–194.e6.

Hepler, C., Shan, B., Zhang, Q., Henry, G.H., Shao, M., Vishvanath, L., Ghaben, A.L., Mobley, A.B., Strand, D., Hon, G.C., and Gupta, R.K. (2018). Identification of functionally distinct fibro-inflammatory and adipogenic stromal subpopulations in visceral adipose tissue of adult mice. eLife *7*, e39636.

Hondares, E., Rosell, M., Díaz-Delfín, J., Olmos, Y., Monsalve, M., Iglesias, R., Villarroya, F., and Giralt, M. (2011). Peroxisome proliferator-activated receptor α (PPARα) induces PPARγ coactivator 1α (PGC-1α) gene expression and contributes to thermogenic activation of brown fat: involvement of PRDM16. J. Biol. Chem. *286*, 43112–43122.

Huang, C.K., Chang, P.H., Kuo, W.H., Chen, C.L., Jeng, Y.M., Chang, K.J., Shew, J.Y., Hu, C.M., and Lee, W.H. (2017). Adipocytes promote malignant growth of breast tumours with monocarboxylate transporter 2 expression via β-hydroxybutyrate. Nat. Commun. *8*, 14706.

Ishibashi, J., and Seale, P. (2015). Functions of Prdm16 in thermogenic fat cells. Temperature (Austin) *2*, 65–72.

Jiang, C., Qu, A., Matsubara, T., Chanturiya, T., Jou, W., Gavrilova, O., Shah, Y.M., and Gonzalez, F.J. (2011). Disruption of hypoxia-inducible factor 1 in adipocytes improves insulin sensitivity and decreases adiposity in high-fat diet-fed mice. Diabetes *60*, 2484–2495.

Joe, A.W., Yi, L., Natarajan, A., Le Grand, F., So, L., Wang, J., Rudnicki, M.A., and Rossi, F.M. (2010). Muscle injury activates resident fibro/adipogenic progenitors that facilitate myogenesis. Nat. Cell Biol. *12*, 153–163.

Kajimura, S., Seale, P., Tomaru, T., Erdjument-Bromage, H., Cooper, M.P., Ruas, J.L., Chin, S., Tempst, P., Lazar, M.A., and Spiegelman, B.M. (2008). Regulation of the brown and white fat gene programs through a PRDM16/CtBP transcriptional complex. Genes Dev. *22*, 1397–1409.

Kajimura, S., Spiegelman, B.M., and Seale, P. (2015). Brown and beige fat: physiological roles beyond heat generation. Cell Metab. *22*, 546–559.

Kennedy, A.R., Pissios, P., Otu, H., Roberson, R., Xue, B., Asakura, K., Furukawa, N., Marino, F.E., Liu, F.F., Kahn, B.B., et al. (2007). A high-fat, ketogenic diet induces a unique metabolic state in mice. Am. J. Physiol. Endocrinol. Metab. *292*, E1724–E1739.

Klingenberg, M., and Huang, S.G. (1999). Structure and function of the uncoupling protein from brown adipose tissue. Biochim. Biophys. Acta *1415*, 271–296.

Lee, Y.H., Petkova, A.P., Mottillo, E.P., and Granneman, J.G. (2012). In vivo identification of bipotential adipocyte progenitors recruited by β3-adrenocceptor activation and high-fat feeding. Cell Metab. *15*, 480–491.

Lee, K.Y., Russell, S.J., Ussar, S., Boucher, J., Vernochet, C., Mori, M.A., Smyth, G., Rourk, M., Cederquist, C., Rosen, E.D., et al. (2013). Lessons on conditional gene targeting in mouse adipose tissue. Diabetes *62*, 864–874.

Lee, Y.H., Petkova, A.P., Konkar, A.A., and Granneman, J.G. (2015). Cellular origins of cold-induced brown adipocytes in adult mice. FASEB J. *29*, 286–299.

Lemos, D.R., Babaeijandaghi, F., Low, M., Chang, C.K., Lee, S.T., Fiore, D., Zhang, R.H., Natarajan, A., Nedospasov, S.A., and Rossi, F.M. (2015). Nilotinib reduces muscle fibrosis in chronic muscle injury by promoting TNF-mediated apoptosis of fibro/adipogenic progenitors. Nat. Med. *21*, 786–794.

Lin, J.Z., Rabhi, N., and Farmer, S.R. (2018). Myocardin-related transcription factor A promotes recruitment of ITGA5+ profibrotic progenitors during obesity-induced adipose tissue fibrosis. Cell Rep. *23*, 1977–1987.

Long, J.Z., Svensson, K.J., Tsai, L., Zeng, X., Roh, H.C., Kong, X., Rao, R.R., Lou, J., Lokurkar, I., Baur, W., et al. (2014). A smooth muscle-like origin for beige adipocytes. Cell Metab. *19*, 810–820.

Lu, Y., Yao, D., and Chen, C. (2013). 2-Hydrazinoquinoline as a derivatization agent for LC-MS-based metabolomic investigation of diabetic ketoacidosis. Metabolites *3*, 993–1010.

Lund, T.M., Obel, L.F., Risa, Ø., and Sonnewald, U. (2011). β-Hydroxybutyrate is the preferred substrate for GABA and glutamate synthesis while glucose is indispensable during depolarization in cultured GABAergic neurons. Neurochem. Int. *59*, 309–318.

Lund, T.M., Ploug, K.B., Iversen, A., Jensen, A.A., and Jansen-Olesen, I. (2015). The metabolic impact of β-hydroxybutyrate on neurotransmission: reduced glycolysis mediates changes in calcium responses and KATP channel receptor sensitivity. J. Neurochem. *132*, 520–531.

Marcelin, G., Ferreira, A., Liu, Y., Atlan, M., Aron-Wisnewsky, J., Pelloux, V., Botbol, Y., Ambrosini, M., Fradet, M., Rouault, C., et al. (2017). A PDGFRα-mediated switch toward CD9^{high} adipocyte progenitors controls obesity-induced adipose tissue fibrosis. Cell Metab. *25*, 673–685.

McDonald, M.E., Li, C., Bian, H., Smith, B.D., Layne, M.D., and Farmer, S.R. (2015). Myocardin-related transcription factor A regulates conversion of progenitors to beige adipocytes. Cell *160*, 105–118.

Merrick, D., Sakers, A., Irgebay, Z., Okada, C., Calvert, C., Morley, M.P., Percec, I., and Seale, P. (2019). Identification of a mesenchymal progenitor cell hierarchy in adipose tissue. Science *364*, eaav2501.

Mullican, S.E., Tomaru, T., Gaddis, C.A., Peed, L.C., Sundaram, A., and Lazar, M.A. (2013). A novel adipose-specific gene deletion model demonstrates potential pitfalls of existing methods. Mol. Endocrinol. *27*, 127–134.

Newman, J.C., and Verdin, E. (2014). Ketone bodies as signaling metabolites. Trends Endocrinol. Metab. *25*, 42–52.

Ohno, H., Shinoda, K., Ohyama, K., Sharp, L.Z., and Kajimura, S. (2013). EHMT1 controls brown adipose cell fate and thermogenesis through the PRDM16 complex. Nature *504*, 163–167.

Ouellet, V., Routhier-Labadie, A., Bellemare, W., Lakhal-Chaieb, L., Turcotte, E., Carpentier, A.C., and Richard, D. (2011). Outdoor temperature, age, sex, body mass index, and diabetic status determine the prevalence, mass, and glucose-uptake activity of 18F-FDG-detected BAT in humans. J. Clin. Endocrinol. Metab. *96*, 192–199.

Pfannenberg, C., Werner, M.K., Ripkens, S., Stef, I., Deckert, A., Schmadl, M., Reimold, M., Häring, H.U., Claussen, C.D., and Stefan, N. (2010). Impact of age on the relationships of brown adipose tissue with sex and adiposity in humans. Diabetes *59*, 1789–1793.

Puchalska, P., and Crawford, P.A. (2017). Multi-dimensional roles of ketone bodies in fuel metabolism, signaling, and therapeutics. Cell Metab. *25*, 262–284.

Puchalska, P., Martin, S.E., Huang, X., Lengfeld, J.E., Daniel, B., Graham, M.J., Han, X., Nagy, L., Patti, G.J., and Crawford, P.A. (2019). Hepatocyte-macrophage acetoacetate shuttle protects against tissue fibrosis. Cell Metab. *29*, 383–398.e7.

Rajakumari, S., Wu, J., Ishibashi, J., Lim, H.W., Giang, A.H., Won, K.J., Reed, R.R., and Seale, P. (2013). EBF2 determines and maintains brown adipocyte identity. Cell Metab. *17*, 562–574.

Ricquier, D. (2011). Uncoupling protein 1 of brown adipocytes, the only uncoupler: a historical perspective. Front. Endocrinol. (Lausanne) *2*, 85.

Rogers, N.H., Landa, A., Park, S., and Smith, R.G. (2012). Aging leads to a programmed loss of brown adipocytes in murine subcutaneous white adipose tissue. Aging Cell *11*, 1074–1083.

Saito, M., Okamatsu-Ogura, Y., Matsushita, M., Watanabe, K., Yoneshiro, T., Nio-Kobayashi, J., Iwanaga, T., Miyagawa, M., Kameya, T., Nakada, K., et al. (2009). High incidence of metabolically active brown adipose tissue in healthy adult humans: effects of cold exposure and adiposity. Diabetes *58*, 1526–1531.

Schwalie, P.C., Dong, H., Zachara, M., Russeil, J., Alpern, D., Akchiche, N., Caprara, C., Sun, W., Schlaudraff, K.U., Soldati, G., et al. (2018). A stromal cell population that inhibits adipogenesis in mammalian fat depots. Nature *559*, 103–108.

Seale, P., Kajimura, S., Yang, W., Chin, S., Rohas, L.M., Uldry, M., Tavernier, G., Langin, D., and Spiegelman, B.M. (2007). Transcriptional control of brown fat determination by PRDM16. Cell Metab. *6*, 38–54.

Seale, P., Bjork, B., Yang, W., Kajimura, S., Chin, S., Kuang, S., Scimè, A., Devarakonda, S., Conroe, H.M., Erdjument-Bromage, H., et al. (2008). PRDM16 controls a brown fat/skeletal muscle switch. Nature *454*, 961–967.

Seale, P., Conroe, H.M., Estall, J., Kajimura, S., Frontini, A., Ishibashi, J., Cohen, P., Cinti, S., and Spiegelman, B.M. (2011). Prdm16 determines the thermogenic program of subcutaneous white adipose tissue in mice. J. Clin. Invest. *121*, 96–105.

Shao, M., Ishibashi, J., Wang, Q., Kusminski, C.M., MacPherson, K.A., Vishvanath, L., Spurgin, S.B., Hepler, C., Holland, W.L., Seale, P., et al. (2016). Conversion of white to beige fat cells and the reversal of obesity through inactivation of adipocyte Zfp423. Cell Metab. *23*, 1167–1184.

Srivastava, S., Kashiwaya, Y., King, M.T., Baxa, U., Tam, J., Niu, G., Chen, X., Clarke, K., and Veech, R.L. (2012). Mitochondrial biogenesis and increased uncoupling protein 1 in brown adipose tissue of mice fed a ketone ester diet. FASEB J. *26*, 2351–2362.

Srivastava, S., Baxa, U., Niu, G., Chen, X., and Veech, R.L. (2013). A ketogenic diet increases brown adipose tissue mitochondrial proteins and UCP1 levels in mice. IUBMB Life *65*, 58–66.

Stine, R., Shapira, S.N., Ishibashi, J., Lim, H.W., Harms, M., Won, K.J., and Seale, P. (2015). EBF2 promotes beige fat cell recruitment in white adipose tissue. Mol. Metab. *5*, 57–65, https://doi.org/10.1016/j.molmet.2015.11.001.

Sun, K., Halberg, N., Khan, M., Magalang, U.J., and Scherer, P.E. (2013a). Selective inhibition of hypoxia-inducible factor 1α ameliorates adipose tissue dysfunction. Mol. Cell. Biol. *33*, 904–917.

Sun, K., Tordjman, J., Clément, K., and Scherer, P.E. (2013b). Fibrosis and adipose tissue dysfunction. Cell Metab. *18*, 470–477.

Trefely, S., Ashwell, P., and Snyder, N.W. (2016). FluxFix: automatic isotopologue normalization for metabolic tracer analysis. BMC Bioinformatics *17*, 485.

Uezumi, A., Fukada, S., Yamamoto, N., Takeda, S., and Tsuchida, K. (2010). Mesenchymal progenitors distinct from satellite cells contribute to ectopic fat cell formation in skeletal muscle. Nat. Cell Biol. *12*, 143–152.

Vanhoutvin, S.A., Troost, F.J., Hamer, H.M., Lindsey, P.J., Koek, G.H., Jonkers, D.M., Kodde, A., Venema, K., and Brummer, R.J. (2009). Butyrate-induced transcriptional changes in human colonic mucosa. PLoS One *4*, e6759.

Vila, I.K., Badin, P.M., Marques, M.A., Monbrun, L., Lefort, C., Mir, L., Louche, K., Bourlier, V., Roussel, B., Gui, P., et al. (2014). Immune cell Toll-like receptor 4 mediates the development of obesity- and endotoxemia-associated adipose tissue fibrosis. Cell Rep. *7*, 1116–1129.

Wang, W., and Seale, P. (2016). Control of brown and beige fat development. Nat. Rev. Mol. Cell Biol. *17*, 691–702.

Wang, Q.A., Tao, C., Gupta, R.K., and Scherer, P.E. (2013). Tracking adipogenesis during white adipose tissue development, expansion and regeneration. Nat. Med. *19*, 1338–1344.

Wang, W., Kissig, M., Rajakumari, S., Huang, L., Lim, H.W., Won, K.J., and Seale, P. (2014). Ebf2 is a selective marker of brown and beige adipogenic precursor cells. Proc. Natl. Acad. Sci. USA *111*, 14466–14471.

Wang, Q., Zhou, Y., Rychahou, P., Fan, T.W., Lane, A.N., Weiss, H.L., and Evers, B.M. (2017). Ketogenesis contributes to intestinal cell differentiation. Cell Death Differ. *24*, 458–468.

Wu, J., Cohen, P., and Spiegelman, B.M. (2013). Adaptive thermogenesis in adipocytes: is beige the new brown? Genes Dev. *27*, 234–250.

Xie, N., Tan, Z., Banerjee, S., Cui, H., Ge, J., Liu, R.M., Bernard, K., Thannickal, V.J., and Liu, G. (2015). Glycolytic reprogramming in myofibroblast differentiation and lung fibrosis. Am. J. Respir. Crit. Care Med. *192*, 1462–1474.

Yoneshiro, T., Aita, S., Matsushita, M., Okamatsu-Ogura, Y., Kameya, T., Kawai, Y., Miyagawa, M., Tsujisaki, M., and Saito, M. (2011). Age-related decrease in cold-activated brown adipose tissue and accumulation of body fat in healthy humans. Obesity (Silver Spring) *19*, 1755–1760.

Zhao, X., Psarianos, P., Soltan Ghoraie, L., Yip, K., Goldstein, D., Gilbert, R., Witterick, I., Pang, H., Hussain, A., Lee, J.H., et al. (2019). Metabolic regulation of dermal fibroblasts contributes to skin extracellular matrix homeostasis and fibrosis. Nat. Metab. *1*, 147–157.

STAR★METHODS

KEY RESOURCES TABLE

REAGENT or RESOURCE	SOURCE	IDENTIFIER
Antibodies		
Rb anti PRDM16	P. Seale	Generated in house
Rb anti PPARg (81B8)	Cell Signaling	Cat# 2443; RRID:AB_823598
Ms anti Tubulin (DM1A)	Sigma	Cat# T6199; RRID:AB_477583
Ms anti Actin, clone C4	Millipore	Cat# MAB1501; RRID:AB_2223041
Ms anti Actin, α-Smooth Muscle	Sigma	Cat# A2547; RRID:AB_476701
Ms anti TGFβ 1, 2, 3	Novus Biologicals	MAB1835; RRID:AB_357931
Ms anti SMAD3	Santa Cruz	Cat# sc-101154; RRID:AB_1129525
Rb anti P-SMAD3	AbCam	Cat# ab52903; RRID:AB_882596
Rb anti HIF1α	Cayman Chemical	Cat# 10006421; RRID:AB_409037
Rb anti Perilipin	Cell Signaling	Cat# 3470, RRID:AB_2167268
Rb anti RFP	VWR Scientific	RL600-401-379
APC anti-mouse PDGFRα	BioLegend	Cat# 135907, RRID:AB_2043969
Goat anti-P-SMAD2/3	Santa-Cruz	Cat# sc-11769, RRID:AB_2193189
Chemicals, Peptides, and Recombinant Proteins		
Tamoxifen (Free Base)	Sigma	T5648
4-hydroxy-tamoxifen	Sigma	H6278
Etomoxir	Sigma	E1905
Corn Oil	Sigma	C8267
Palmitic Acid	Sigma	76119
Methanol (HPLC)	VWR	MX0475-1
Water (HPLC)	Fisher Chemical	W5-1
Palmitic Acid [9,10-3H(N)], 1mCi	Perkin Elmer	NET043001MC
DMOG	Cayman Chemical	71210
Recombinant Mouse TGFβ	R & D	7345-B2
ion-exchange columns	Bio-Rad	7316211
Palmitic Acid (1-13C, 99%)	Cambridge Isotopes	CLM-150
Sodium-3-hydroxybutyrate	Sigma	54965
TruSeq RNA Sample Prep Kit v2 set A	Illumina	RS-122-2001
PCR Master Mix, Power SYBR Green	Applied Biosystems	4367659
CL 316, 243	Sigma	C5976
Deposited Data		
RNA sequencing data -Young versus Aged mice (+/− CL316,243) -Control (Puro) versus PRDM16-expressing adipose cells	GEO repository	GSE129083 GSE129084
Experimental Models: Organisms/Strains		
R26^{CreER}	The Jackson Laboratory	004847
Prdm16 ^{flox}	The Jackson Laboratory	024992
Bdh1 ^{flox}	Dr. Daniel Kelly	N/A
Adipoq^{Cre}	The Jackson Laboratory	010803
Rosa26^{tdTomato}	The Jackson Laboratory	007914
Pdgfr$\alpha^{creERT2}$	Dr. Brigid Hogan	N/A
Adipoq^{rtTA}	Dr. Philipp Scherer	N/A
Tre^{Cre}	The Jackson Laboratory	006234
Rosa26^{mTmG}	The Jackson Laboratory	007676

Continued

REAGENT or RESOURCE	SOURCE	IDENTIFIER
Prdm16-deficient	Dr. Patrick Seale	N/A
Fabp4-Prdm16	Dr. Bruce Spiegelman	N/A
Oligonucleotides		
See Table S1 for qPCR Primers	Integrated DNA Technologies (IDT)	N/A
Recombinant DNA		
PLKO.1-shRNA-Scramble	Addgene,Sabatini, PMID15718470	1864
PLKO.1-shRNA-Bdh1	The RNAi Consortium (TRC)- Broad Institute via UPenn High-Throughput Screening Core	TRCN0000041898
pMD2.G	Addgene (Gift from Didier Trono)	12259
psPAX2	Addgene (Gift from Didier Trono)	12260
LentiCRISPR v2	Addgene (Gift from Feng Zhang)	52961
MSCV-GFP	Dr. Patrick Seale	N/A
MSCV-Prdm16	Dr. Patrick Seale	N/A
Software and Algorithms		
GraphPad Prism 7	GraphPad Software	https://www.graphpad.com/scientific-software/prism/
ImageJ	NIH	https://imagej.nih.gov/ij/
R	Open source	https://www.r-project.org/
GSEA	Broad Institute	http://software.broadinstitute.org/gsea/index.jsp
Reactome (Pathway Browser)	PMID: 29145629	https://reactome.org/PathwayBrowser/

CONTACT FOR REAGENT AND RESOURCE SHARING

Further information and requests for resources and reagents should be directed to and will be fulfilled by the Lead Contact, Patrick Seale (sealep@pennmedicine.upenn.edu).

EXPERIMENTAL MODEL AND SUBJECT DETAILS

Mice

All animal experiments were approved by the University of Pennsylvania's Institutional Animal Care and Use Committee. Mice were housed in temperature-controlled, pathogen-free barrier facility on a 12 hr/12 hr light/dark cycle. 12-month-old C57BL/6 male mice were obtained from the National Institute of Aging. *Adipoq^{Cre}* (strain name: B6; FVB-Tg(Adipoq-cre)1Evdr/J, stock no. 010803), *Rosa26^{tdTomato}* (strain name: B6.Cg-Gt(ROSA)26Sortm14(CAG-tdTomato)Hze/J, stock no. 007914), *Rosa26^{CreER}* (strain name: B6;129-Gt(ROSA)26Sortm1(cre/ERT)Nat/J, stock no. 004847) mouse strains were obtained from the Jackson Laboratory. *Prdm16$^{flox/flox}$*, *Fabp4-Prdm16* and *Prdm16*-deficient mice were generated as described previously (Cohen et al., 2014; Harms et al., 2014; Seale et al., 2008, 2011). The *Adipoq^{rtTA}*; *TRE^{Cre}*; *Rosa26$^{mT/mG}$* *AdipoChaser* mice were described before (Shao et al., 2016; Wang et al., 2013). The *Pdgfrα^{creERT2}* mouse strain was obtained from Dr. Brigid Hogan (Duke University). *Bdh1^{flox}* mice were obtained from Dr. Dan Kelly (University of Pennsylvania). All mouse strains were maintained on a C57BL/6J background. Sibling or age matched male mice were used for all the experiments. To induce Cre activity, tamoxifen (Sigma, T5648) was dissolved at 20 mg/mL in corn oil (Sigma, C8267) and 5-7 weeks old mice were intraperitoneally injected with tamoxifen at a dose of 100 mg/kg for 5 consecutive days. Mice were then scarified at the specific days following the last tamoxifen injection. For CL 316,243 (Sigma, C5976) treatment, mice were intraperitoneally injected with 1 mg/kg CL 316,243 for 5 consecutive days. For *in vivo* etomoxir (Sigma, E1905) treatment, mice were intraperitoneally injected with 45 mg/kg etomoxir for 5 consecutive days. For cold exposure, mice were singly housed at 5 C for 7 days.

Cell Culture

Primary inguinal progenitors were isolated from 7-12 weeks old male mice as previously described (Wang et al., 2014). Briefly, inguinal adipose tissues were dissected, minced into small pieces (approximate 1 cm^3 in size) with scissors. Minced samples were then transferred to the DMEM/F12 media containing 1.5 U/ ml collagenase D (Sigma, 11088858001) and 2.4 U/mL Dispase (Sigma, 4942078001) and rotated for 45 min at 37 C. Digested samples were then passed over a 100-μM filter to remove undigested clump, and stromal cells were gently pelleted. Stromal cells were resuspended in DMEM/F12 media containing 100 μg/mL primocin

(Invivogen, ant-pm-2), and 10% fetal bovine serum (FBS). Cells were induced to undergo adipocyte differentiation using a standard cocktail (DMEM/F12 containing 10% FBS, 0.5 μM isobutylmethylxanthine, 125 nM indomethacin, 1 μM dexamethasone, 20 nM insulin, 1 nM T3, and 1 μM rosiglitazone). After 48 hr, cells were switched to maintenance medium (DMEM/F12 containing 10% FBS, 20 nM insulin, 1 nM T3, and 1 μM rosiglitazone). To delete *Prdm16* in adipocytes, primary inguinal preadipocytes were isolated from *Rosa26*^{CreER}; *Prdm16*^{flox/flox} mice, and then treated with 1 μM 4-hydroxy-tamoxifen (Sigma, H6278) for 3 days in growth phase. For CRISPR/Cas9-mediated gene editing, guide RNA sequences against *Hif1α* or the *Rosa26* gene (negative control) were cloned into LentiCRISPR (R, Addgene, 49535). The following retroviral cDNA constructs were used for gain-of-function studies: MSCV-puro, MSCV-GFP, MSCV-PRDM16, MSCV-HIF1αP577A/P402A (generously provided by Dr. Celeste Simon). To activate HIF1α, cells were treated with 250 μM (high dose) or 100 μM (low dose) of Dimethyloxaloylglycine (DMOG, Cayman Chemical, 71210). For Oil-Red-O staining, cells were fixed with 4% paraformaldehyde (PFA), washed with water twice, followed by 60% isopropanol for 5 min at room temperature (RT). Then, cells were stained with oil red o (Sigma, O0625) at RT for 10 min. For LipidTOX staining, cells were fixed with 4% PFA, and stained with lipidTOX (Thermo Scientific, H34476) at RT for half an hour.

To prepare conditioned medium (CM), cells were incubated with 4 mL of DMEM/F12 (with 10% dialyzed FBS or 200 μM palmitic acid) for 24 hr. CM was then collected, centrifuged at 1000xg for 10 min at 4°C, and the supernatant stored at −80°C. For charcoal purification, CM was incubated with 1% (w/v) activated charcoal (Sigma, 05105) at room temperature for 10 min, and then centrifuged at 1000xg for 15 min to remove charcoal. To study the effects of the FAO inhibitor, etomoxir (Sigma, E1905), on CM activity, "secretor" cells were treated with 25 μM etomoxir for 24 hr.

METHOD DETAILS

ACTA2/SMA Staining and Morphological Analysis in Cultured Cells
Cells were trypsinized, counted and plated (3 X 10^4 cells per well) on chamber slides in the presence or absence of CM or BHB. After 2 h, cells were treated with 500 μM DMOG for another 24 h. Cells were then fixed in 4% paraformaldehyde (PFA) in PBS for 15 min, and permeabilized with 0.4% Triton X-100 in PBS for 15 min. Cells were then stained with SMA antibody (Sigma, A2547). Cell images were captured at low magnification (20 X objective) with a Leica TCS SP8 Confocal. Fluorescence intensity was quantified by using the morphology analysis tools available in the ImageJ software.

Mass Spectrometry-Based SCFA Measurements
SCFAs were measured in conditioned media and tissue extracts by LC-MS after derivitization with 2-hydrazinoquinoline (Lu et al., 2013). $^{13}C_4$-D-β-hydroxybutyrate and $^{13}C_2{}^2H_3$-acetate (both from Cambridge Isotope laboratories) internal standards were added to a media samples to a final concentration of 1 mM (for ^{13}C tracing experiments, only $^{13}C_2{}^2H_3$-acetate was used as an internal standard). Standard curves for were generated by serial dilution of pure standards (β-hydroxybutyrate and $^{13}C_4$-β-hydroxybutyrate (Sigma)) and internal standard was added to standard curve samples in the same manner as to the media samples. For derivitization, 5 μl of sample was combined with 50 μl of acetonitrile containing 2 mM triphenylphosphine (TPP) and 2 mM 2,2-dipyridyl disulfide (DPDS), followed by the addition of 50 μl of acetonitrile containing 2 mM 2-hydrazinoquinoline in a screw cap glass tube. The reaction was incubated at 60°C for 15 min after which, samples were placed on ice and the reaction was stopped by the addition of 100 μL of HPLC (Optima) grade water. Samples were centrifuged at 2000 x g at 4°C for 10 min and the upper 100 μL of cleared supernatant was taken for LC-MS analysis. Samples were separated on a UHPLC BEH C18 column (2.1 × 50 mm) attached to an Acquity LC system (Waters). Solvents were - A: 0.05% aqueous acetic acid containing 2 mM ammonium acetate, and B: 95% aqueous acetonitrile containing 0.05% acetic acid and 2 mM ammonium acetate. Samples were run over a 5 min gradient with starting conditions 1% solvent B ramping to 100% B over 1 min and held at 100% B for 2.5 min before re-equilibration at 1% B for 1.5 min. LC eluate was analyzed with a TSQ triple-quadrupole mass spectrometer (Thermo) with positive electrospray ionization. Data were acquired by selected reaction monitoring of the mass transitions indicted in the table below.

Metabolite	Parent ion [M+H]	Product ions
Acetate	202	143, 160
13C2-Acetate	204	143, 160
13C2,2H3-Acetate	207	143, 160
β-hydroxybutyrate	246	143, 160
13C4-β-hydroxybutyrate	250	143, 160

SCFA Extraction from Frozen Tissues
Frozen tissue samples were cut to ~20 mg on a super chilled ceramic tile on dry ice and the weight of each piece was recorded. Tissues were extracted in 200 μL 80:20 methanol:water chilled to −80°C in a 1.5 mL plastic tube. Ball bearings (2 per sample) were added and tissues were homogenized by mechanical disruption in a bullet blender (Next Advance) operated at intensity 11 for 5 min at 4°C. Samples were centrifuged at 17,000 x g for 10 min at 4°C and the cleared supernatant was used for SCFA determination.

In Vitro Isotopic Labeling

Adipocyte cultures were washed with PBS twice, and then incubated with 4 mL DMEM/F12 (no FBS) containing 100 μM U-$^{13}C_{16}$-Palmitate or unlabeled Palmitate. After 1hr or 6hr incubation, cell culture dishes were placed on ice. 1 mL fresh medium was added to an empty well without any cells as a blank control. Medium was collected, and centrifuged at 1000 x g for 10 min at 4°C. The supernatant was subjected to MS analysis. Cells were washed with ice cold PBS three times, and then harvested in 1 mL 10% (w/v) ice cold trichloroacetic acid for acyl-CoA extraction. Total protein levels were used for normalization.

Water-Soluble Metabolite Extraction

Adipocyte cultures were washed with ice cold PBS twice, and then harvested in ice cold methanol (HPLC) on dry ice. After 20 min of incubation at −80°C, the resulting mixture was collected and centrifuged at 16000 x g for 5 min. The pellets were re-extracted with 1 mL ice cold methanol on dry ice. The supernatants from two rounds of extraction were combined, dried under nitrogen, and subjected to MS analysis. Total protein levels were used for normalization.

Acyl-CoA Extraction and Measurement

Acyl-CoAs were extracted from ∼20 mg frozen tissue pieces into 1 mL 10%(w/v) ice cold trichloroacetic acid with $^{13}C_3{}^{15}N_1$-labeled acyl-CoA internal standard and purified by solid phase extraction as described previously (Frey et al., 2016). Acyl-CoAs were detected on a Q-Exactive (Thermo) mass spectrometer as described previously (Frey et al., 2016). For isotopic tracer analysis, isotopic enrichment was calculated to compensate for the non-linearity of isotopic enrichment using the FluxFix calculator (Trefely et al., 2016).

Flow Cytometry

Isolated cells were filtered through 100 μm and 40 μm filters (Corning), and then incubated with the RBC lysis buffer at RT for 5 min, and then washed with PBS. Cells were stained with antibodies at 1:200 dilution in FACS buffer (HBSS with 3% FBS) for 30 min at 4°C and sorted using a BD FACS Aria. Debris and dead cells were excluded by forward scatter, side scatter, and DAPI gating.

Ketone Ester (KE) Feeding

Animals were provided with a complete liquid diet once per day. Control diet was prepared at 226 g/L Control Liquid Diet powder (Bio-Serv, F1259SP) and supplemented with 2.0 g/L acesulfame K (Sigma, 04054) artificial sweetener and 0.1 mL/L food-grad pure mint extract (McCormick, MD). An isocaloric 6% ketone ester (KE) diet was prepared with 38.3 g/L control diet powder, 187.7 g/L ethanol diet powder, 240 mL/L of 25% ketone ester, plus acesulfame K and mint extract. Animals were housed singly to monitor food consumption. All mice were initially ad-lib fed with control diet to adapt them to liquid diet. The mass of diet consumed was measured each day, and the amount provided to the control group was matched to the amount eaten by the "KE" group during the previous day (pair-feeding). Body masses and food consumption were monitored daily in the morning (∼10-12 AM), and fresh food provided in the afternoon (∼4-6 PM). The mice were maintained on KE and CTL diet for 30 days, followed by a 4-day cold exposure to elicit beiging. Blood samples were collected, mice were euthanized, and tissues were collected and frozen in liquid nitrogen.

Fatty Acid Oxidation Assay

Cells were incubated in DMEM/F12 supplemented with [9,10-^{3}H(N)]palmitate conjugated on BSA and carnitine for 2 hr. The resultant ^3H_2O in the incubation solution was separated using ion-exchange columns (Bio Rad, #7316211), and then measured by scintillation counter. Total protein levels were used for normalization.

RNA-seq and Analysis

RNA-seq libraries were generated with the illumina Truseq RNA Sample Preparation kit (Version 2, Illumina, RS-122-2001). High-throughput sequencing were performed on the HiSeq2000 at the Next Generation Sequencing Core at the University of Pennsylvania. RNA-seq reads were aligned to mm9 using STAR pipeline (R). Genes with fold-changes > 2, and FDR < 0.01 were selected for gene ontology analysis. Gene Set Enrichment Analysis (GSEA) was performed using the Molecular Signatures Database (MSigDB) C2 collection of cellular processes. For GSEA, RNA-seq data was first ranked according to the FDR to generate an ordered gene list for Pre-ranked GSEA.

Histology

For immunohistochemistry, isolated tissues were fixed in 4% PFA overnight, dehydrated, and embedded in paraffin for sectioning. Following de-paraffinization, slides were stained with hematoxylin and eosin, Masson's Trichrome stain or picro-sirius red (abcam, ab150681). For immunostaining, heat antigen retrieval was performed in a pressure cooker using Bulls Eye Decloaking buffer (Bio-care). Slides were incubated in primary antibody overnight followed by multiple washes with PBS. Sections were then incubated with secondary antibody conjugated to peroxidase and developed using Tyramide Signal Amplification (TSA, Perkin Elmer). The following primary antibodies were used: UCP1 (generously provided by AstraZeneca), PLIN1 (Cell Signaling, 3470S), RFP (VWR Scientific, RL600-401-379). Images were captured on a Leica TCS SP8 confocal microscope or a Keyence BZ-X700 fluorescent light microscope.

QPCR and Western Blot

Total RNA was extracted by TRIzol (Invitrogen) followed by purification using PureLink RNA columns (Invitrogen). Isolated mRNA was reverse transcribed using the High-Capacity cDNA Synthesis kit (Applied Biosystems) and used in real-time PCR reactions with SYBR Green master mix (Applied Biosystems) on a 7900 HT (Applied Biosystems). *Tata-binding protein* (*Tbp*) was used an internal normalization control. Primer sequences are in Table S1. Protein extracts were prepared as previously described (Rajakumari et al., 2013). Cells or tissues were lysed in radioimmunoprecipitation assay (RIPA) lysis buffer containing 0.5% NP-40, 0.1% sodium deoxycholate, 150 mM NaCl, 50 mM Tris-Cl, pH 7.5, protease inhibitor cocktail (Complete; Roche) and 1 mM phenylmethylsulfonyl fluoride (PMSF). The protein content was measured using a detergent-compatible (DC) protein assay kit (Bio-Rad). Lysates or nuclear fractions were resolved onto bis-Tris NuPAGE gels (Invitrogen), transferred to PVDF membrane (Millipore). For HIF1α western blot, 500 μM DMOG was freshly added to lysis buffer to prevent HIF1α degradation. Primary antibodies were: anti-PRDM16 (Seale et al., 2007), anti-PPARγ (Cell Signaling Technology, 81b8), anti-UCP1 (R&D Systems, MAB6158), anti-HIF1α (Cayman Chemical, 10006421), anti-Actin (Millipore, MAB1501), anti-TGFβ (Novus Biologicals, MAB1835), anti-P-Smad3 (AbCam, ab52903), anti-Smad3 (Santa Cruz, sc-101154)

QUANTIFICATION AND STATISTICAL ANALYSIS

Unless specified in the main test or figure legends, all sample numbers (n) represent biological replicates. For analysis of the statistical significance of difference between two or three groups, two-sided unpaired Student's t test was used. For analysis of the statistical significance of difference between four or more groups, two-way ANOVA was used All data are shown as the mean with SEM No samples or animals were excluded from analysis. Sample size estimation was not used. Studies were not conducted blinded.

DATA AND SOFTWARE AVAILABILITY

The Gene Expression Omnibus (GEO) accession numbers for the RNA sequencing data reported in this paper are as follows: GSE129083 for datasets comparing young and aged inguinal WAT with our without CL316,243 treatment; and GSE129084 for datasets comparing vehicle control versus PRDM16-expressing adipose cells.